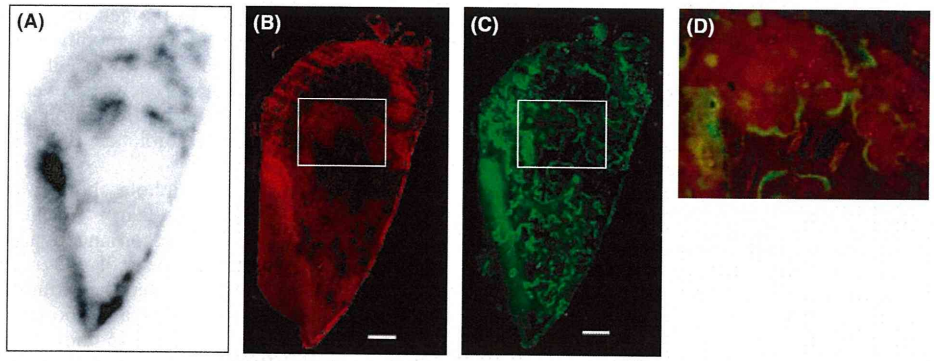

Fig. 3. Representative images of an autoradiogram (A), hypoxia-inducible factor (HIF)-1α immunostaining (B), and pimonidazole immunostaining (C) in the identical section. A high-magnification merged image of HIF-1α immunostaining with pimonidazole immunostaining (D, from insets in B,C) shows that some regions were positive for both stains (yellow) but others did not overlap (red or green). Bars = 1 mm (B,C).

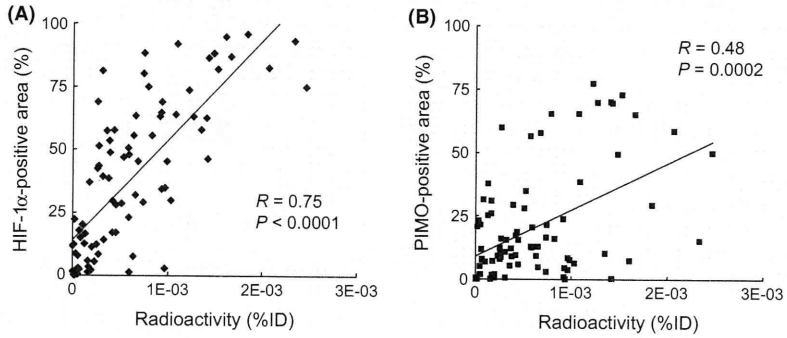

Fig. 4. Correlation between the intratumoral distribution of [^{125}I]IPOS and the level of hypoxia-inducible factor (HIF)-1α expression (A) or that of pimonidazole (PIMO)-adduct formation (B). The ordinate represents the percentage of HIF-1α- and PIMO-positive areas in each region of interest (ROI), and the abscissa represents [^{125}I]IPOS accumulation (%ID) in the same ROI. A total of 10 sections (two sections per tumor) were analyzed. Regression analysis of the areas showing [^{125}I]IPOS accumulation with HIF-1α- or PIMO-positive areas reveal a significantly positive correlation in both cases (HIF-1α: $R = 0.75$, $P < 0.0001$; PIMO: $R = 0.48$, $P = 0.0002$). The results of the chi-square-test reveal that the correlation coefficient between [^{125}I]IPOS and HIF-1α was significantly higher than that between [^{125}I]IPOS and PIMO ($P < 0.01$).

performance due to difficulties in attenuation and scattering correction, and the sensitivity of multi-pinhole SPECT is still lower than PET. However, because SPECT can theoretically achieve a higher spatial resolution than PET, wherein the resolution is limited by the positron range, it is suitable for small animal imaging. In fact, several multi-pinhole SPECT systems are able to image small components within mouse organs.[31,32] The *in vivo* images obtained in the present study were consistent with the results of *ex vivo* biodistribution. The tumor was clearly visualized, but no accumulation of radioactivity was observed in the opposite leg (Fig. 1A,B,D), indicating a high tumor/muscle ratio (10 in *ex vivo* biodistribution). Our observation of high radioactivity in the bladder (Fig. 1E) was in accordance with the finding that the radioactivity was mainly excreted in urine after the administration of [^{125}I]IPOS.

The characterization of [^{125}I]IPOS has been reported in a previous study.[14] Although the tumor uptake of [^{125}I]IPOS was significantly and positively correlated with HIF-1 transcriptional activity, suggesting the feasibility of [^{125}I]IPOS as an HIF-1-active tumor imaging probe, a direct comparison between the intratumoral distribution of [^{125}I]IPOS and HIF-1 expression has not yet been carried out. In the present study, the majority of the [^{125}I]IPOS-distributed areas in the tumor corresponded to HIF-1α-positive hypoxic areas, although there were a few unmatched regions (Fig. 3). A significant positive correlation was observed between the areas, and the correlation coefficient between [^{125}I]IPOS and HIF-1α was significantly greater than that between [^{125}I]IPOS and PIMO (Fig. 4). Although we cannot exclude the effect of the difference in the molecular sizes of [^{125}I]IPOS and PIMO on the distribution, these findings are consistent with the results of recent studies showing that HIF-1α-positive areas are not always colocalized with PIMO-positive areas.[33–35] Thus, [^{125}I]IPOS can be viewed as a probe that depicts HIF-1-active areas rather than the physically hypoxic areas themselves.

Although the detailed mechanism of cellular uptake and retention of [^{125}I]IPOS is now under investigation, we found that low temperature (4°C) or ATP depletion inhibited the cellular uptake of [^{125}I]IPOS (unpublished data). As most studies have shown endocytosis as the major cellular uptake pathway for most PTDs[36,37] and endocytosis occurs in an energy-dependent manner, [^{125}I]IPOS is probably uptaken by the cells through the endocytotic pathway. After uptake by endocytosis, [^{125}I]IPOS could be released from the endosomes and retained intracellularly because of its molecular size. In fact, in our previous experiment, [^{125}I]IPOS was not cleared from the cells under hypoxic conditions for at least 24 h, after the incubation medium was replaced with fresh medium.[14] Although the intracellular radioactivity decreased gradually under normoxic conditions, the cleared radioactivity was mainly attributable to the small molecules.[14] These findings indicated the intracellular retention ability of [^{125}I]IPOS.

doi: 10.1111/j.1349-7006.2011.02057.x

In the present study, the biodistribution of [^{125}I]IPOS was consistent with a previous report;[14] thus, the reproducibility of the biodistribution of [^{125}I]IPOS was confirmed. Although the amount of tumoral accumulation of [^{125}I]IPOS was not as high as that of 2-[^{18}F]fluoro-2-deoxy-D-glucose ([^{18}F]FDG), this could have been due to the limited expression of HIF-1. The expression of HIF-1 is not ubiquitous, but heterogeneous, and is small in tumors.[6] In fact, the probe accumulation in the tumors harboring HIF-1-dependent reporter genes was 1–2%ID/g in previous studies,[6,38,39] which is comparable to the results of the present study. The size-exclusion analysis revealed that the radioactivity in the tumor existed as 34-kDa macromolecules that were most likely [^{125}I]IPOS existing stably in hypoxic regions. Furthermore, the radioactivity in urine and feces were mainly in low-molecular-weight compounds. This was consistent with our previous *in vitro* findings showing that [^{125}I]IPOS was degraded in normoxic cells and that [^{125}I]IBB and other small molecules were cleared from the cells.[14] Thus, these findings prove the concept of [^{125}I]IPOS *in vivo* and show that [^{125}I]IPOS exists stably only in the HIF-1-active regions while undergoing degradation and clearance in normoxic regions.

Although HIF-1α was reported to degrade within a few minutes under normoxic conditions,[5] the degradation of [^{125}I]IPOS was relatively slow.[14] Thus, a long exposure time is necessary to obtain sufficiently contrasting images; this is one of the drawbacks of [^{125}I]IPOS. Moreover, a study has shown that the acute hypoxic region created by the shutdown of blood vessels can be reoxygenated after reopening the blood vessels.[40] In such reoxygenated areas especially, the inconsistency in the rates of degradation of HIF-1α and [^{125}I]IPOS may be responsible for the differences in the distribution pattern of [^{125}I]IPOS and HIF-1α expression. POS comprises not only the ODD, which is the essential domain related to oxygen-dependent degradation, but also the PTD and SAV. This modification may hamper the degradation of the probe. However, this is not a substantial problem; a pretargeting approach can overcome this drawback. In fact, a 4–8-fold earlier visualization of the tumor can be achieved with the SAV–radiolabeled biotin-based pretargeting approach.[15,18]

In conclusion, multi-pinhole high-resolution SPECT/CT imaging with [^{125}I]IPOS clearly visualized a tumor. The obtained images were in accordance with the corresponding autoradiograms and the analysis of *ex vivo* biodistribution. The autoradiograms documented that the intratumoral distribution of [^{125}I]IPOS was heterogeneous and showed a good correlation with HIF-1α-positive areas. These findings indicate that the distribution of [^{125}I]IPOS reflects the expression of HIF-1α, thus rendering [$^{123/125}$I]IPOS an effective probe for the molecular imaging of HIF-1-active tumors.

Acknowledgments

This work was supported in part by "R&D of Molecular Imaging Equipment for Malignant Tumor Therapy Support" by the New Energy and Industrial Technology Development Organization, Japan, a Health Labour Sciences Research Grant for Research on Advanced Medical Technology from the Ministry of Health, Labour and Welfare of Japan, and a Grant-in-Aid for Exploratory Research (17659010) and a Grant-in-Aid for Young Scientists (B) (21791187) from the Ministry of Education, Culture, Sports, Science and Technology of Japan.

Disclosure Statement

The authors have no conflict of interest.

References

1 Kizaka-Kondoh S, Konse-Nagasawa H. Significance of nitroimidazole compounds and hypoxia-inducible factor-1 for imaging tumor hypoxia. *Cancer Sci* 2009; **100**: 1366–73.
2 Zhong H, De Marzo AM, Laughner E *et al.* Overexpression of hypoxia-inducible factor 1alpha in common human cancers and their metastases. *Cancer Res* 1999; **59**: 5830–5.
3 Semenza GL. Targeting HIF-1 for cancer therapy. *Nat Rev Cancer* 2003; **3**: 721–32.
4 Schwartz DL, Powis G, Thitai-Kumar A *et al.* The selective hypoxia inducible factor-1 inhibitor PX-478 provides in vivo radiosensitization through tumor stromal effects. *Mol Cancer Ther* 2009; **8**: 947–58.
5 Kizaka-Kondoh S, Tanaka S, Harada H, Hiraoka M. The HIF-1-active microenvironment: an environmental target for cancer therapy. *Adv Drug Deliv Rev* 2009; **61**: 623–32.
6 Serganova I, Doubrovin M, Vider J *et al.* Molecular imaging of temporal dynamics and spatial heterogeneity of hypoxia-inducible factor-1 signal transduction activity in tumors in living mice. *Cancer Res* 2004; **64**: 6101–8.
7 Lecomte R. Novel detector technology for clinical PET. *Eur J Nucl Med Mol Imaging* 2009; **36** (Suppl 1): S69–85.
8 Lewellen TK. Recent developments in PET detector technology. *Phys Med Biol* 2008; **53**: R287–317.
9 Riemann B, Schafers KP, Schober O, Schafers M. Small animal PET in preclinical studies: opportunities and challenges. *Q J Nucl Med Mol Imaging* 2008; **52**: 215–21.
10 Rowland DJ, Cherry SR. Small-animal preclinical nuclear medicine instrumentation and methodology. *Semin Nucl Med* 2008; **38**: 209–22.
11 Wang GL, Jiang BH, Rue EA, Semenza GL. Hypoxia-inducible factor 1 is a basic-helix-loop-helix-PAS heterodimer regulated by cellular O_2 tension. *Proc Natl Acad Sci USA* 1995; **92**: 5510–4.
12 Choi HJ, Song BJ, Gong YD, Gwak WJ, Soh Y. Rapid degradation of hypoxia-inducible factor-1alpha by KRH102053, a new activator of prolyl hydroxylase 2. *Br J Pharmacol* 2008; **154**: 114–25.
13 Kizaka-Kondoh S, Itasaka S, Zeng L *et al.* Selective killing of hypoxia-inducible factor-1-active cells improves survival in a mouse model of invasive and metastatic pancreatic cancer. *Clin Cancer Res* 2009; **15**: 3433–41.
14 Kudo T, Ueda M, Kuge Y *et al.* Imaging of HIF-1-active tumor hypoxia using a protein effectively delivered to and specifically stabilized in HIF-1-active tumor cells. *J Nucl Med* 2009; **50**: 942–9.
15 Ueda M, Kudo T, Kuge Y *et al.* Rapid detection of hypoxia-inducible factor-1-active tumours: pretargeted imaging with a protein degrading in a mechanism similar to hypoxia-inducible factor-1alpha. *Eur J Nucl Med Mol Imaging* 2010; **37**: 1566–74.
16 Ueda M, Iida Y, Tominaga A *et al.* Nicotinic acetylcholine receptors expressed in the ventralposterolateral thalamic nucleus play an important role in anti-allodynic effects. *Br J Pharmacol* 2010; **159**: 1201–10.
17 Temma T, Ogawa Y, Kuge Y *et al.* Tissue factor detection for selectively discriminating unstable plaques in an atherosclerotic rabbit model. *J Nucl Med* 2010; **51**: 1979–86.
18 Kudo T, Ueda M, Konishi H *et al.* PET imaging of hypoxia-inducible factor-1-active tumor cells with pretargeted oxygen-dependent degradable streptavidin and a novel (18)F-labeled biotin derivative. *Mol Imaging Biol* 2010; 10.1007/s11307-010-0418-6 [Epub ahead of print].
19 Motta-Hennessy C, Sharkey RM, Goldenberg DM. Metabolism of indium-111-labeled murine monoclonal antibody in tumor and normal tissue of the athymic mouse. *J Nucl Med* 1990; **31**: 1510–9.
20 Postema EJ, McEwan AJ, Riauka TA *et al.* Initial results of hypoxia imaging using 1-alpha-D-(5-deoxy-5-[^{18}F]-fluoroarabinofuranosyl)-2-nitroimidazole (^{18}F-FAZA). *Eur J Nucl Med Mol Imaging* 2009; **36**: 1565–73.
21 Dunphy MP, Lewis JS. Radiopharmaceuticals in preclinical and clinical development for monitoring of therapy with PET. *J Nucl Med* 2009; **50** (Suppl 1): 106S–21S.
22 Krohn KA, Link JM, Mason RP. Molecular imaging of hypoxia. *J Nucl Med* 2008; **49** (Suppl 2): 129S–48S.
23 Jiang BH, Semenza GL, Bauer C, Marti HH. Hypoxia-inducible factor 1 levels vary exponentially over a physiologically relevant range of O_2 tension. *Am J Physiol* 1996; **271**: C1172–80.
24 Yeom CJ, Chung JK, Kang JH *et al.* Visualization of hypoxia-inducible factor-1 transcriptional activation in C6 glioma using luciferase and sodium iodide symporter genes. *J Nucl Med* 2008; **49**: 1489–97.
25 He F, Deng X, Wen B *et al.* Noninvasive molecular imaging of hypoxia in human xenografts: comparing hypoxia-induced gene expression with endogenous and exogenous hypoxia markers. *Cancer Res* 2008; **68**: 8597–606.

26 Carlin S, Pugachev A, Sun X *et al.* In vivo characterization of a reporter gene system for imaging hypoxia-induced gene expression. *Nucl Med Biol* 2009; **36**: 821–31.
27 Harada H, Kizaka-Kondoh S, Itasaka S *et al.* The combination of hypoxia-response enhancers and an oxygen-dependent proteolytic motif enables real-time imaging of absolute HIF-1 activity in tumor xenografts. *Biochem Biophys Res Commun* 2007; **360**: 791–6.
28 Moroz E, Carlin S, Dyomina K *et al.* Real-time imaging of HIF-1alpha stabilization and degradation. *PLoS One* 2009; **4**: e5077.
29 Kuchimaru T, Kadonosono T, Tanaka S, Ushiki T, Hiraoka M, Kizaka-Kondoh S. In vivo imaging of HIF-active tumors by an oxygen-dependent degradation protein probe with an interchangeable labeling system. *PLoS One* 2010; **5**: e15736.
30 Grassi R, Cavaliere C, Cozzolino S *et al.* Small animal imaging facility: new perspectives for the radiologist. *Radiol Med* 2009; **114**: 152–67.
31 Pissarek M, Meyer-Kirchrath J, Hohlfeld T *et al.* Targeting murine heart and brain: visualisation conditions for multi-pinhole SPECT with (99m)Tc- and (123)I-labelled probes. *Eur J Nucl Med Mol Imaging* 2009; **36**: 1495–509.
32 van der Have F, Vastenhouw B, Ramakers RM *et al.* U-SPECT-II: an ultra-high-resolution device for molecular small-animal imaging. *J Nucl Med* 2009; **50**: 599–605.
33 Lehmann S, Stiehl DP, Honer M *et al.* Longitudinal and multimodal in vivo imaging of tumor hypoxia and its downstream molecular events. *Proc Natl Acad Sci U S A* 2009; **106**: 14004–9.
34 Li XF, Carlin S, Urano M, Russell J, Ling CC, O'Donoghue JA. Visualization of hypoxia in microscopic tumors by immunofluorescent microscopy. *Cancer Res* 2007; **67**: 7646–53.
35 Sobhanifar S, Aquino-Parsons C, Stanbridge EJ, Olive P. Reduced expression of hypoxia-inducible factor-1alpha in perinecrotic regions of solid tumors. *Cancer Res* 2005; **65**: 7259–66.
36 Madani F, Lindberg S, Langel U, Futaki S, Graslund A. Mechanisms of cellular uptake of cell-penetrating peptides. *J Biophys* 2011; **2011**: 414729.
37 Nakase I, Takeuchi T, Tanaka G, Futaki S. Methodological and cellular aspects that govern the internalization mechanisms of arginine-rich cell-penetrating peptides. *Adv Drug Deliv Rev* 2008; **60**: 598–607.
38 Hsieh CH, Kuo JW, Lee YJ, Chang CW, Gelovani JG, Liu RS. Construction of mutant TKGFP for real-time imaging of temporal dynamics of HIF-1 signal transduction activity mediated by hypoxia and reoxygenation in tumors in living mice. *J Nucl Med* 2009; **50**: 2049–57.
39 Wen B, Burgman P, Zanzonico P *et al.* A preclinical model for noninvasive imaging of hypoxia-induced gene expression; comparison with an exogenous marker of tumor hypoxia. *Eur J Nucl Med Mol Imaging* 2004; **31**: 1530–8.
40 Kizaka-Kondoh S, Inoue M, Harada H, Hiraoka M. Tumor hypoxia: a target for selective cancer therapy. *Cancer Sci* 2003; **94**: 1021–8.

doi: 10.1111/j.1349-7006.2011.02057.x

Cancer Science
The official journal of the Japanese Cancer Association

Development of membrane type-1 matrix metalloproteinase-specific activatable fluorescent probe for malignant tumor detection

Yoichi Shimizu, Takashi Temma, Kohei Sano, Masahiro Ono and Hideo Saji[1]

Department of Patho-Functional Bioanalysis, Graduate School of Pharmaceutical Sciences, Kyoto University, Kyoto, Japan

(Received February 15, 2011/Revised June 13, 2011/Accepted June 20, 2011/Accepted manuscript online June 30, 2011/Article first published online July 29, 2011)

Membrane type-1 matrix metalloproteinase (MT1-MMP) is a protease that activates pro-MMP-2 and pro-MMP13, which are related to tumor malignancy. Therefore, probes that specifically image MT1-MMP would be useful for malignant tumor diagnosis. In the present study, we prepared rhodamine X-conjugated anti-MT1-MMP antibody (anti-MT1-MMP mAb-ROX) as an activatable fluorescent probe and evaluated its usefulness for MT1-MMP-specific imaging. Anti-MT1-MMP mAb-ROX was obtained in a quenched form with approximately three ROX molecules per mAb. Its fluorescence intensity increased approximately 14-fold in the presence of detergent, which is suitable for activatable systems. C6 glioma cells and MCF-7 human breast adenocarcinoma cells were used as MT1-MMP-positive and MT1-MMP-negative models, respectively. The fluorescence intensity of C6 cells treated with anti-MT1-MMP mAb-ROX, but not ROX-conjugated isotype control antibody (NC Ab-ROX), increased with time and was significantly higher than that of MCF-7 cells at 6 h ($P < 0.001$). The fluorescence intensity of cells treated with anti-MT1-MMP mAb-ROX was also suppressed by pre-treatment with a MT1-MMP endocytosis inhibitor ($P < 0.05$). Furthermore, the probes were intravenously administered to C6 and MCF-7 xenografted mice. The tumor-to-muscle (T/M) ratio of the anti-MT1-MMP mAb-ROX group was 15.1 ± 3.2 at 48 h and was significantly higher than that of the NC Ab-ROX group (T/M ratio = 4.6 ± 3.0, $P < 0.05$) in C6 xenografted mice, while the T/M ratio of the anti-MT1-MMP mAb-ROX and NC Ab-ROX groups was not different in MCF-7 xenografted mice. These findings suggest that anti-MT1-MMP mAb-ROX is a promising probe for specifically detecting MT1-MMP-expressing tumors. (*Cancer Sci* 2011; 102: 1897–1903)

Cancer is a major cause of mortality and morbidity in the world and its incidence continues to increase. Although conventional treatment options have advanced significantly, they remain far from optimal due to ineffective diagnosis. Accordingly, effective methods for detecting malignant tumors in their early stages are needed for successful therapy.[1,2]

Matrix metalloproteinases (MMP) are a family of zinc-binding, calcium-dependent proteolytic enzymes that can remodel the extracellular matrix (ECM) as well as cleave a number of cell surface modulators associated with several pathological conditions.[3–6] In humans, the MMP family includes 16 secreted MMP and seven membrane-associated MMP (MT-MMP).[7] Among the MMP, MT1-MMP (MMP-14) not only promotes tumor growth and ECM proteolysis, but also activates pro-MMP-2 and pro-MMP-13 on the cell surface, especially at lamellipodia, the migration front of cells.[8] Therefore, MT1-MMP has a close relationship with tumor malignancy and holds great promise as an early biomarker for malignant tumors.[9,10]

Currently, optical imaging techniques using target-specific probes are of great interest.[11–16] As such, we aimed to develop a MT1-MMP-specific activatable probe that couples the fluorescent label rhodamine X (ROX) to an anti-MT1-MMP monoclonal antibody (anti-MT1-MMP mAb-ROX). This probe can be obtained in a self-quenched form, and on specific interaction with MT1-MMP expressed on the surface of malignant cells the probe is internalized by the cell and is subsequently degraded by the lysosome,[17] which dequenches the probe fluorescence allowing optical signal emission.[17] This sequence follows a mechanism similar to that in a report describing the development of ROX-labeled avidin for use in optical imaging of a wide range of tumors.[11] Thus, anti-MT1-MMP mAb-ROX might permit estimation of tumor malignancy.

In the present study, we prepared anti-MT1-MMP mAb-ROX and evaluated its effectiveness as a specific imaging probe for MT1-MMP-expressing tumors by characterizing cellular uptake and probe biodistribution in C6-implanted mice.

Materials and Methods

Preparation of anti-MT1-MMP mAb-ROX. All chemicals were commercially available and of the highest purity. Anti-MT1-MMP mAb (113-5B7, mouse IgG_3; Daiichi Fine Chemical Co., Ltd, Toyama, Japan), a purified mouse monoclonal antibody for residues 319–333 (numbered with respect to the signal peptide) of human MT1-MMP was used after further purification on a HiTrap rProtein A column (GE Healthcare, UK Ltd, Buckinghamshire, UK). 5-(and-6)-Carboxy-X-Rhodamine (20 μg; Invitrogen, Carlsbad, CA, USA) in DMSO (2 μL) was added to the anti-MT1-MMP mAb solution in 0.02 M Na_2HPO_4 (250 μL, 2 mg/mL). After stirring with light protection for 15 min at room temperature, the mixture was purified on a Sephadex G-25 column (PD-10; GE Healthcare, UK Ltd) equilibrated with 0.1 M PBS (pH 7.4) to obtain anti-MT1-MMP mAb-ROX. The concentrations of the protein and ROX were determined by absorption at 280 and 584 nm, respectively. The molar extinction coefficient of antibody and ROX were 165 000 and 42 400/M/cm respectively.

Sodium dodecyl sulfate polyacrylamide gel electrophoresis (SDS-PAGE) was performed as previously described.[18] Mouse immunoglobulin G_3, kappa mAb (ab18392; Abcam, Cambridge, UK) was labeled with ROX in a similar way to obtain a negative control (NC Ab-ROX).

Determination of fluorescent property. To determine the effect of dequenching, anti-MT1-MMP mAb-ROX (2.3 μg/mL) and NC Ab-ROX (2.3 μg/mL) were incubated in 1 mL PBS (0.1 M, pH 7.4) with or without 5% SDS for 30 min at room temperature. After incubation, fluorescence emission spectra were measured with a fluorescence spectrometer (RF-5300; SHIMADZU Corporation, Kyoto, Japan), following excitation at 580 nm.

[1]To whom correspondence should be addressed.
E-mail: hsaji@pharm.kyoto-u.ac.jp

doi: 10.1111/j.1349-7006.2011.02020.x

Determination of immunoreactivity. The immunoreactivity of anti-MT1-MMP mAb-ROX was evaluated as previously described.[19] In brief, anti-MT1-MMP mAb, anti-MT1-MMP mAb-ROX and NC Ab were radiolabeled with ^{125}I using the chloramine T method and then added to mouse macrophage cells (RAW264.7, 2.5×10^6 to 2×10^7 cells) suspended in 0.01 M PBS (pH 7.4, 100 μL), followed by incubation for 30 min at 4°C. After centrifugation, the radioactivity of the pellets and supernatants was measured with a gamma counter (1470 WIZARD; PerkinElmer Japan Co., Osaka, Japan). The percentage of antibody bound to cells (% Bound) was calculated using the following equation:

$$\%\,\text{Bound} = \frac{\text{Radioactivity of pellets}}{\text{Radioactivity of pellets and supernatants}} \times 100$$

Cellular uptake study. C6 glioma cells (HSRRB, Tokyo, Japan) and MCF-7 human breast adenocarcinoma cells (ATCC, Manassas, VA, USA) were cultured in DMEM medium with 10% fetal bovine serum at 37°C in a humidified atmosphere containing 5% CO_2. After pre-incubation on a glass-bottom dish for 16 h, anti-MT1-MMP mAb-ROX or NC Ab-ROX (10 μg/1 mL DMEM) was added to the cells (2×10^5 cells) and incubated at 37°C in a humidified atmosphere containing 5% CO_2. At 30 min, 1, 3 and 6 h, cells were washed twice with PBS, incubated with Hoechst 33342 (1 μg/mL) for 1 min, and washed twice again. The cells were examined by fluorescence microscopy (BIOREVO BZ9000; Keyence Japan Co., Osaka, Japan) using the following filters: excitation wavelength, 540–580 nm (for ROX), 340–380 nm (for Hoechst 33342); and emission wavelength, 600–660 nm (for ROX), 435–485 nm (for Hoechst 33342). The fluorescence intensity was analyzed with BZ-II Analyzer 1.10 software (Keyence Japan Co.).

For the blocking study, C6 cells were treated with type I collagen (Col I; 100 μg/1 mL DMEM) for 24 h at 37°C.[20] The cells were washed twice with PBS, and anti-MT1-MMP mAb-ROX (10 μg/1 mL DMEM) was added. After incubation for 30 min, 1, 3 and 6 h at 37°C in a humidified atmosphere containing 5% CO_2, cells were washed twice, incubated with Hoechst 33342 (1 μg/mL) for 1 min, washed twice again, and fluorescence microscopy studies were performed as described above.

***In vivo* biodistribution study.** Female Balb/c *nu/nu* mice (7 weeks old) and female SCID mice (5 weeks old), supplied by Japan SLC, Inc. (Hamamatsu, Japan) and CLEA Japan, Inc. (Tokyo, Japan), respectively, were housed under a 12-h light/12-h dark cycle and given free access to food and water. The animal experiments were conducted in accordance with institutional guidelines and approved by the Kyoto University Animal Care Committee. C6 or MCF-7 cells were suspended in 0.1 M PBS (pH 7.4) followed by subcutaneous inoculation into the right hind leg of Balb/c *nu/nu* mice (1×10^7 cells/100 μL PBS/mouse) or SCID mice (2×10^7 cells/100 μL PBS/mouse), respectively. Tumor volume was estimated by ([length] × [width]^2)/2 over a 14–16-day (C6 xenografted mice) or 45-day (MCF-7 xenografted mice) period.

Animals were divided into three groups ($n = 3$ in each group) for three time points with approximately equal distribution of tumor sizes on the day before the study. After the mice were killed at 1, 24 and 48 h post-administration of anti-MT1-MMP mAb-ROX or NC Ab-ROX (40 μg/100 μL PBS) via tail vein, each organ was excised and weighed. Fluorescence images of organs were acquired with an IVIS SPECTRUM imaging system (Caliper Life Sciences Inc., Hopkinton, MA, USA) with a 1-s exposure (f-stop = 4) and a customized filter set (excitation, 560–580 nm; emission, 630–650 nm). The fluorescence intensity in each region of interest covering an entire tissue was expressed as photons/sec per g after the subtraction of background signal obtained in a region of interest set over an area without any tissue. The tissue-to-muscle and tissue-to-blood fluorescence intensity ratios were then calculated.

Statistics. Data are represented as mean ± SD. Statistical analyses of *in vitro* and *in vivo* studies were performed with two-way factorial ANOVA followed by the Tukey–Kramer test, with the exception of comparison between C6 and MCF-7 groups in the cellular uptake study with unpaired Student's *t*-test.

Results

Preparation of anti-MT1-MMP mAb-ROX. The number of ROX per anti-MT1-MMP mAb molecule was 3.1 ± 0.4 ($n = 15$). In the SDS-PAGE analysis of purified anti-MT1-MMP mAb-ROX, the fluorescent signal of ROX was observed on a band close to the 150 kDa molecular weight marker, confirming that ROX was indeed conjugated to the antibody (Fig. 1).

Characterization of anti-MT1-MMP mAb-ROX. Figure 2 shows the fluorescence emission spectra of anti-MT1-MMP mAb-ROX, which was obtained in a quenched form (dashed line). The fluorescence intensity increased ~14-fold in the presence of 5% SDS (bold line) to a level similar to that produced by ROX alone (dotted line).

Figure 3 shows the binding of [^{125}I] anti-MT1-MMP mAb, [^{125}I] anti-MT1-MMP mAb-ROX and [^{125}I] NC Ab-ROX to RAW264.7 cells as a function of cell number. [^{125}I] anti-MT1-MMP mAb and [^{125}I] anti-MT1-MMP mAb-ROX showed similar curves ($P = 0.363$ by two factor factorial ANOVA), which increased with cell number. In contrast, [^{125}I] NC Ab exhibited low binding over the range of estimation, indicating that anti-MT1-MMP mAb-ROX retained immunoreactivity similar to that of the anti-MT1-MMP mAb.

Cellular uptake study. Serial observation of C6 cells (showing high MT1-MMP expression determined by western blotting [Data S1 and Fig. S1]) incubated with anti-MT1-MMP mAb-ROX or NC Ab-ROX was performed using fluorescence microscopy for 6 h to compare the change in intracellular fluorescence intensity (Fig. 4A). The fluorescence intensity of cells treated with anti-MT1-MMP mAb-ROX increased in a time-dependent manner and was significantly higher than that of cells treated with NC Ab-ROX ($P < 0.05$ and $P < 0.01$ at 3 and 6 h, respectively; Fig. 4B). The cells treated with NC Ab-ROX showed negligibly low fluorescence for 6 h. The fluorescence intensity of MCF-7 cells (showing low MT1-MMP expression determined by western blotting [Fig. S1]) was also significantly low ($P < 0.001$; Fig. 5).

In addition, when cells were pretreated with the endocytosis inhibitor Col I, the fluorescence intensity of cells incubated with anti-MT1-MMP mAb-ROX was significantly depressed to 43.7% of the non-pretreated group at 6 h ($P < 0.05$; Fig. 6).

***In vivo* studies.** The values of the main organ at each time point were acquired as total fluorescence flux per organ weight (photon/sec per g; the one example of an acquired image of the organs of C6 xenografted mice at 48 h after administration of anti-MT1-MMP mAb-ROX is shown in Fig. S2), and tissue-to-muscle ratios were then calculated (Table 1). For C6 xenografted mice, tumor-to-muscle (T/M) ratios increased in a manner similar to the fluorescence intensity in tumors. The T/M ratios obtained were 9.6 ± 2.5 and 15.1 ± 3.2 at 24 and 48 h post-injection of anti-MT1-MMP mAb-ROX, respectively, which was significantly higher than those at 24 and 48 h after injection of NC Ab-ROX (2.6 ± 0.6 and 4.6 ± 3.0, respectively; $P < 0.05$). We also calculated the tumor-to-blood (T/B) ratios in the same manner as the T/M ratios. The T/B ratio at 48 h after injection of anti-MT1-MMP mAb-ROX was also significantly higher than that of animals treated with NC Ab-ROX for

doi: 10.1111/j.1349-7006.2011.02020.x

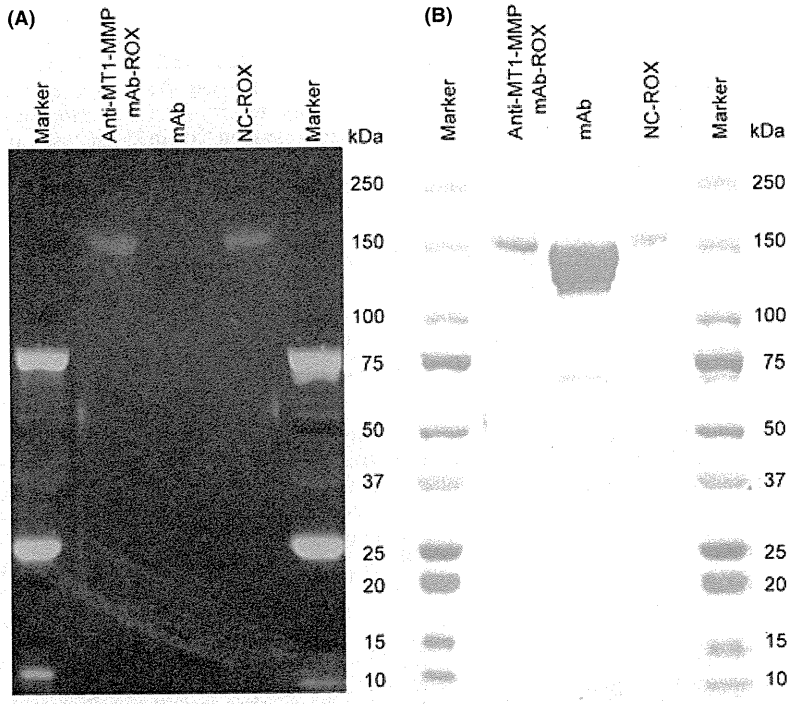

Fig. 1. CBB stains (A) and fluorescent images (B) of anti-membrane type-1 matrix metalloproteinase (MT1-MMP) mAb-rhodamine X (ROX) after electrophoresis.

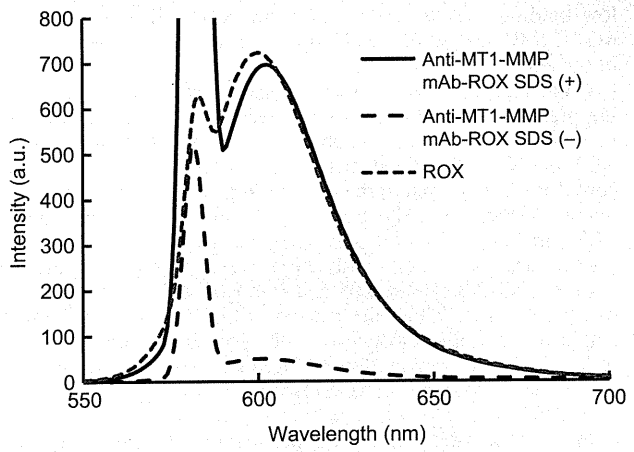

Fig. 2. Fluorescence emission spectra of anti-membrane type-1 matrix metalloproteinase (MT1-MMP) mAb-rhodamine X (ROX) after incubation with 5% SDS (anti-MT1-MMP mAb-ROX SDS[+]) (bold line) or without 5% SDS (anti-MT1-MMP mAb-ROX SDS[–]) (dashed line) for 30 min and that of ROX alone (dotted line). These samples were excited at 580 nm.

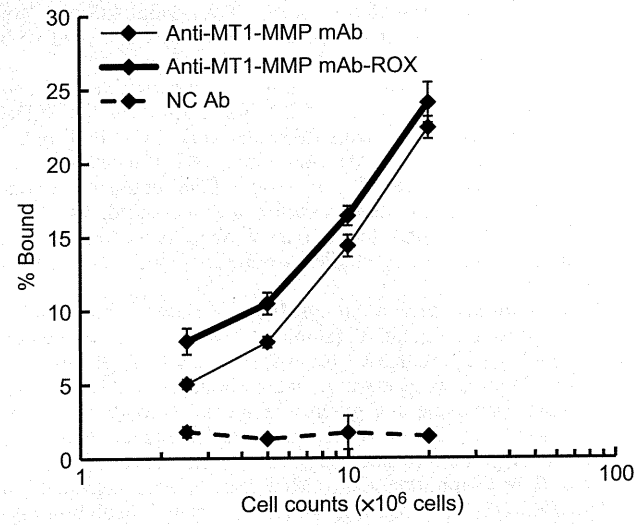

Fig. 3. Radioactivity of radiolabelled anti-membrane type-1 matrix metalloproteinase (MT1-MMP) mAb (solid line), anti-MT1-MMP mAb-rhodamine X (ROX) (bold line) and NC Ab (dotted line) bound to mouse macrophages (RAW264.7). Data are expressed as % Bound (mean ± SD) for three samples. The difference among the time-courses was estimated by two factor factorial ANOVA.

48 h (48.9 ± 13.5 *vs* 11.1 ± 3.7; $P < 0.01$). In contrast, the T/M ratios of MCF-7 xenografted mice were 5.2 ± 1.6 and 8.9 ± 1.9 at 24 and 48 h post-injection of anti-MT1-MMP mAb-ROX, respectively, which were not different from those at 24 and 48 h post-injection of NC Ab-ROX (5.3 ± 1.6 and 10.9 ± 0.6, respectively).

Discussion

In the present study, we developed an activatable-type fluorescence probe, anti-MT1-MMP mAb-ROX. Anti-MT1-MMP mAb-ROX was dramatically activated under antibody-degeneration conditions (Fig. 2), and in stained C6 cells (Fig. 4). Activation of anti-MT1-MMP mAb-ROX was not seen in the negative control MCF-7 cells (Fig. 5). Changes in fluorescence could be blocked by pretreating C6 cells with an endocytosis inhibitor (Fig. 6). These results serve as proof of concept for the development of fluorescence probes having a monoclonal antibody core structure and having the specificity, selectivity and high

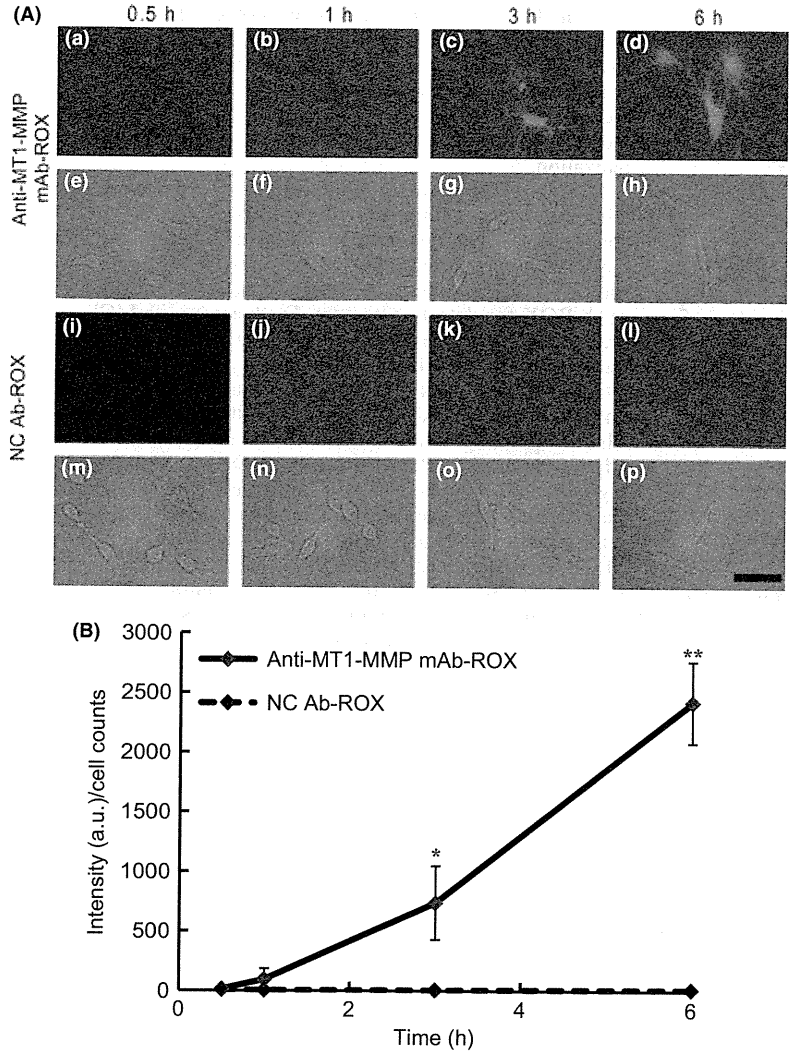

Fig. 4. (A) Fluorescent (a–d, i–l) and bright-field (e–h, m–p) microscopy images of C6 glioma cells at 0.5 h (a,e,i,m), 1 h (b,f,j,n), 3 h (c,g,k,o) and 6 h (d,h,l,p) after the addition of anti-membrane type-1 matrix metalloproteinase (MT1-MMP) mAb-rhodamine X (ROX) (a–h) or NC Ab-ROX (i–p). Bar, 40 μm. (B) The mean fluorescence intensity (600–660 nm) of C6 cells at 0.5, 1, 3 and 6 h after incubation with anti-MT1-MMP mAb-ROX (solid line) or NC-ROX (dotted line). Data are expressed as fluorescence intensity per cell counts (mean ± SD) for 4–5 samples. Comparison between the anti-MT1-MMP mAb-ROX-treated group and the NC Ab-ROX-treated group was performed with two-way factorial ANOVA followed by Tukey–Kramer test (*$P < 0.05$, **$P < 0.01$ *vs* NC Ab-ROX).

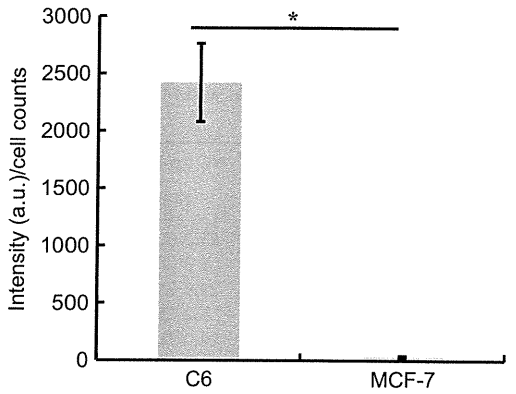

Fig. 5. The mean fluorescence intensity (600–660 nm) of C6 cells and MCF-7 cells at 6 h after incubation with anti-membrane type-1 matrix metalloproteinase (MT1-MMP) mAb-rhodamine X (ROX). Data are expressed as fluorescence intensity per cell counts (mean ± SD) for 3–4 samples. Comparison between C6 and MCF-7 cell groups was performed with unpaired Student's *t*-test (*$P < 0.001$ *vs* MCF-7).

sensitivity necessary to target molecules. In addition, high T/M and T/B ratios were observed in tumor-bearing mice expressing MT1-MMP (Table 1), suggesting that our probe would be clinically useful for *in vivo* imaging of MT1-MMP expressed in malignant tumors.

We used ROX as the fluorophore for the MT1-MMP specifically activatable fluorescence probe. Rhodamine derivatives bound to proteins have been reported to form H-dimers easily at low concentrations,[21] which might cause self-quenching, and fluorescence activation can be triggered on unfolding and degeneration of the rhodamine-conjugated protein. Because MT1-MMP expressed at the cell surface is known to be internalized and delivered to the lysosome for degradation,[17] this strategy would be suitable for MT1-MMP-specific activatable fluorescence imaging.

A variety of malignant tumors such as breast cancer, glioma and fibrosarcoma are reported to express MT1-MMP.[22–24] In the present study, we used C6 glioma cells that express MT1-MMP at high levels[25] and MCF-7 human breast adenocarcinoma cells that show low MT1-MMP expression as model cell lines for evaluating the efficacy of our probe. Preliminary *in vitro* studies using the cell lines MDA-MB-231 and HT1080 derived from human blastoma and human fibrosarcoma,

doi: 10.1111/j.1349-7006.2011.02020.x

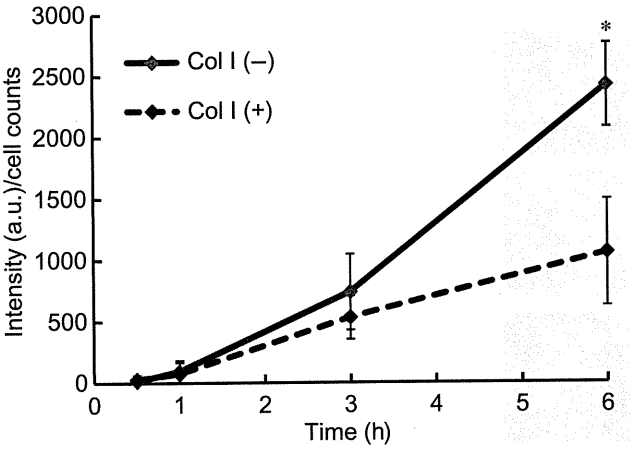

Fig. 6. The mean fluorescence intensity (600–660 nm) of C6 cells treated with (dotted line) or without (solid line) Col I for 24 h at 0.5, 1, 3 and 6 h after incubation with anti-membrane type-1 matrix metalloproteinase (MT1-MMP) mAb-rhodamine X (ROX). Data are expressed as fluorescence intensity per cell counts (mean ± SD) for 3–4 samples. Comparisons between the Col I-treated group (Col I [+]) and the Col I-untreated group (Col I [–]) were performed with two-way factorial ANOVA followed by Tukey–Kramer test (*$P < 0.05$ *vs* Col I [+]).

respectively, indicate that this probe will also be suitable for these types of tumors (data not shown). The fluorescence in C6 cells treated with anti-MT1-MMP mAb-ROX gradually increased with time and was significantly observed from 3 h post-incubation. This time-course seems rather long compared with radiolabeled anti-MT1-MMP mAb in our previous study.[26] However, considering that MT1-MMP expressed on the cell surface is reportedly internalized to the endosome and eventually recycled to the cell surface within 1 h,[27] it would be expected that anti-MT1-MMP mAb-ROX would require additional time to emit a fluorescent signal following its degeneration in cells.

To further verify the fluorescence emission mechanism, we next planned an *in vitro* inhibition study using Col I, which has been shown to be an inhibitor of dynamin-dependent MT1-MMP internalization.[20,28,29] Pretreatment of cells with Col I significantly depressed the fluorescence intensity of the probe as expected. The moderate fluorescent signal observed in cells pretreated with Col I might be due to other internalization processes, such as clathrin-independent mechanisms involving caveolae, which also process MT1-MMP in addition to dynamin-dependent internalization in tumor cells.[20,29,30] Considering these aspects, MT1-MMP imaging in the present study was indeed achieved by activation after MT1-MMP-dependent internalization.

In C6 glioma xenografted mice, the T/M ratios increased with time after administration of anti-MT1-MMP mAb-ROX and the ratios were significantly higher than those of the NC Ab-ROX-treated group ($P < 0.01$ estimated by two-way factorial ANOVA), indicating the effectiveness of anti-MT1-MMP mAb-ROX for detecting tumors. Furthermore, in MCF-7 xenografted mice there was no difference between the T/M ratios of the anti-MT1-MMP mAb-ROX-treated group and those of the NC Ab-ROX-treated group. This result would support that anti-MT1-MMP mAb-ROX can specifically visualize MT1-MMP-expressing tumors. In addition, the T/B ratio of mice administered anti-MT1-MMP mAb-ROX was also significantly higher than that of the NC Ab-ROX group at 48 h after administration, although the fluorescent signals in blood would be diminished by endogenous fluorophores such as hemoglobin.[31] The high T/B ratio of anti-MT1-MMP mAb-ROX might again support the strategy of the probe. In contrast, NC Ab-ROX showed moderate accumulation of fluorescence in tumors, which we also observed in our previous study using radiolabelled MT1-MMP mAb.[26] While this result could be due to the enhanced permeability and retention (EPR) effect,[32] the contrast of T/B ratios between anti-MT1-MMP mAb and NC Ab nevertheless was improved for the activatable fluorescence probe compared with the RI probe (approximately 4 at anti-MT1-MMP mAb-ROX/NC Ab-ROX versus approximately 1.5 at ^{99m}Tc-anti-MT1-MMP mAb/^{99m}Tc-NC Ab[26]). This discrepancy between optical and RI probes could be derived from differences in signal controllability *in vivo*. In other words, nuclear imaging probes cannot be signal-activatable type for *in vivo* usage, unlike the optical imaging probes prepared in this paper. Although macromolecular probes without any targeting moieties, such as antibodies, liposomes and micelles, accumulate in tumors by the EPR effect; the accumulation site is at first in interstitial spaces in the tumors, followed by slow non-specific internalization into the tumor cells.[33] As the macromolecule probes with targeting moieties attach to the tumor cells for active entry, the quantity and rate for the accumulation inside the tumor cells might increase naturally. Importantly, in the case of signal-activatable type optical probes like anti-MT1-MMP

Table 1. Biodistribution of fluorescence intensity per organ weight (x10^7 photon/sec per g) after injection of anti-MT1-MMP mAb-ROX or NC Ab-ROX in Balb/c *nu/nu* mice bearing C6 rat glioma tumors

Tissue	Anti-MT1-MMP mAb ROX			NC Ab-ROX		
	1 h	24 h	48 h	1 h	24 h	48 h
Liver	42.6 (1.7)	17.6 (3.1)	17.0 (5.0)	68.2 (10.2)	25.2 (2.7)	14.3 (6.4)
Kidney	10.5 (2.4)	12.0 (2.9)	13.9 (4.8)	24.1 (10.5)	8.9 (4.3)	1.9 (1.1)
Pancreas	18.3 (12.6)	23.8 (7.1)	30.7 (5.2)	39.5 (6.5)	29.9 (9.9)	23.0 (19.3)
Spleen	17.8 (2.2)	7.0 (3.3)	6.5 (2.2)	25.5 (9.4)	5.2 (0.9)	4.8 (6.2)
Heart	10.1 (7.6)	4.3 (1.0)	3.6 (2.8)	10.6 (4.9)	4.0 (2.6)	3.1 (1.8)
Lung	42.7 (18.9)	19.7 (8.4)	14.2 (3.1)	47.7 (1.6)	23.6 (6.5)	13.9 (8.3)
Brain	17.6 (5.0)	16.3 (1.0)	15.7 (1.4)	23.0 (4.2)	13.5 (1.9)	9.7 (6.0)
Muscle	7.5 (4.0)	5.5 (2.3)	4.0 (1.5)	8.4 (1.0)	13.0 (1.9)	9.0 (6.0)
Tumor	27.2 (5.9)	48.4 (11.6)	64.2 (16.4)	13.1 (1.5)	34.2 (13.1)	26.9 (12.9)
Tumor/muscle	5.1 (3.0)	9.6 (2.5)	15.1 (3.2)	1.6 (0.2)	2.6 (0.6)	4.6 (3.0)
Liver/muscle	8.5 (5.4)	3.9 (2.5)	3.9 (3.2)	8.3 (2.0)	2.0 (0.1)	1.9 (0.7)
Kidney/muscle	2.0 (1.4)	2.6 (1.0)	3.2 (1.7)	3.0 (1.4)	0.7 (0.2)	0.2 (0.04)

Each value represents the mean (±SD) for three animals. MMP, matrix metalloproteinase; MT1, membrane type-1; ROX, rhodamine X.

mAb-ROX, there is a lower signal (ideally negligible signals) in the interstitial space because the probes emit optical signals only after internalization to the tumor cells. In contrast, a relatively higher signal in the interstitial space is inevitable in the case of radioactive antibody probes. Taken together, the improvement of the contrast between anti-MT1-MMP mAb and NC Ab-ROX compared with the RI probe contributes to the signal-activatable ability of our probe. Therefore, anti-MT1-MMP mAb-ROX would be superior for MT1-MMP-expressing tumor imaging applications.

Several MT1-MMP imaging probes have been developed for use with single photon emission computed tomography (SPECT) and fluorescence imaging.[34–37] These probes used MT1-MMP substrate as a basic structure, and showed good imaging *in vitro*. However, some of these substrates were also recognized by other MMP subtypes such as MMP-2, because the amino acid sequences of these substrates are not completely specific to MT1-MMP, and as such would produce non-specific signals. In contrast, the anti-MT1-MMP monoclonal antibody we selected for the basic structure in the present study possesses both high specificity[38] and affinity (sub-nanomolar K_d value in our preliminary data) for MT1-MMP, providing strict imaging of malignant tumors expressing MT1-MMP.

However, the fluorescence wavelength of our probe was too short for detection from outside the body because light in the near-infrared (NIR) region (700–1000 nm) is appropriate with respect to tissue permeability.[31,39,40] Provided that a NIR fluorophore is introduced to the probe to satisfy the strategy for MT1-MMP-specific activation, this could be a useful alternative for *in vivo* optical imaging in the future. Fluorescence endoscopy imaging technology has been rapidly advancing and is expected to provide a navigation system for surgery.[41,42] For endoscopy, fluorescence probes emitting light in the visible region are suitable because most targets exist at shallow tissue depths and require visibility rather than permeability of fluorescence emitted from a probe. Like a variety of probes,[9,14,15,21] the anti-MT1-MMP mAb-ROX (fluorescence around 600 nm) that we developed could thus also be an appropriate choice for diagnosing tumor malignancy using fluorescence endoscopic technology.

In conclusion, we synthesized an anti-MT1-MMP mAb-ROX that specifically interacts with MT1-MMP expressed on tumor cells and is internalized by these cells and its fluorescence dequenched after antibody unfolding and degeneration. The results indicate that anti-MT1-MMP mAb-ROX would be a useful probe for detecting MT1-MMP-expressing tumors.

Acknowledgments

A part of this study was conducted as a part of the project, ''R&D Project on Molecular Imaging Equipment/Development of Core Technology on Novel Molecular Imaging Probes for Malignant Tumor Detection/Development of Elemental Technology for Molecular Imaging Probes'', supported by the New Energy and Industrial Technology Development Organization (NEDO), Japan.

Disclosure Statement

The authors have no conflict of interest.

References

1 Gindy ME, Prud'homme RK. Multifunctional nanoparticles for imaging, delivery and targeting in cancer therapy. *Expert Opin Drug Deliv* 2009; **6**: 865–78.
2 Alford R, Ogawa M, Choyke PL, Kobayashi H. Molecular probes for the *in vivo* imaging of cancer. *Mol Biosyst* 2009; **5**: 1279–91.
3 Egeblad M, Werb Z. New functions for the matrix metalloproteinases in cancer progression. *Nat Rev Cancer* 2002; **2**: 161–74.
4 Lafleur MA, Handsley MM, Edwards DR. Metalloproteinases and their inhibitors in angiogenesis. *Expert Rev Mol Med* 2003; **5**: 1–39.
5 Overall CM, Lopez-Otin C. Strategies for MMP inhibition in cancer: innovations for the post-trial era. *Nat Rev Cancer* 2002; **2**: 657–72.
6 Kuge Y, Takai N, Ishino S, Temma T, Shiomi M, Saji H. Distribution profiles of membrane type-1 matrix metalloproteinase (MT1-MMP), matrix metalloproteinase-2 (MMP-2) and cyclooxygenase-2 (COX-2) in rabbit atherosclerosis: comparison with plaque instability analysis. *Biol Pharm Bull* 2007; **30**: 1634–40.
7 Page-McCaw A, Ewald AJ, Werb Z. Matrix metalloproteinases and the regulation of tissue remodelling. *Nat Rev Mol Cell Biol* 2007; **8**: 221–33.
8 Mori H, Tomari T, Koshikawa N *et al.* CD44 directs membrane-type 1 matrix metalloproteinase to lamellipodia by associating with its hemopexin-like domain. *EMBO J* 2002; **21**: 3949–59.
9 Jones JL, Glynn P, Walker RA. Expression of MMP-2 and MMP-9, their inhibitors, and the activator MT1-MMP in primary breast carcinomas. *J Pathol* 1999; **189**: 161–8.
10 Knauper V, Bailey L, Worley JR, Soloway P, Patterson ML, Murphy G. Cellular activation of proMMP-13 by MT1-MMP depends on the C-terminal domain of MMP-13. *FEBS Lett* 2002; **532**: 127–30.
11 Hama Y, Urano Y, Koyama Y *et al.* A target cell-specific activatable fluorescence probe for *in vivo* molecular imaging of cancer based on a self-quenched avidin-rhodamine conjugate. *Cancer Res* 2007; **67**: 2791–9.
12 Bremer C, Tung CH, Weissleder R. *In vivo* molecular target assessment of matrix metalloproteinase inhibition. *Nat Med* 2001; **7**: 743–8.
13 Kamiya M, Kobayashi H, Hama Y *et al.* An enzymatically activated fluorescence probe for targeted tumor imaging. *J Am Chem Soc* 2007; **129**: 3918–29.
14 Ogawa M, Kosaka N, Longmire MR, Urano Y, Choyke PL, Kobayashi H. Fluorophore-quencher based activatable targeted optical probes for detecting *in vivo* cancer metastases. *Mol Pharm* 2009; **6**: 386–95.
15 Urano Y, Asanuma D, Hama Y *et al.* Selective molecular imaging of viable cancer cells with pH-activatable fluorescence probes. *Nat Med* 2009; **15**: 104–9.
16 Mahmood U, Tung CH, Bogdanov A Jr, Weissleder R. Near-infrared optical imaging of protease activity for tumor detection. *Radiology* 1999; **213**: 866–70.
17 Osenkowski P, Toth M, Fridman R. Processing, shedding, and endocytosis of membrane type 1-matrix metalloproteinase (MT1-MMP). *J Cell Physiol* 2004; **200**: 2–10.
18 Aita K, Temma T, Shimizu Y, Kuge Y, Seki K, Saji H. Synthesis of a new NIR fluorescent Nd complex labeling agent. *J Fluoresc* 2010; **20**: 225–34.
19 Arano Y, Wakisaka K, Ohmono Y *et al.* Assessment of radiochemical design of antibodies using an ester bond as the metabolizable linkage: evaluation of maleimidoethyl 3-(tri-n-butylstannyl)hippurate as a radioiodination reagent of antibodies for diagnostic and therapeutic applications. *Bioconjug Chem* 1996; **7**: 628–37.
20 Lafleur MA, Mercuri FA, Ruangpanit N, Seiki M, Sato H, Thompson EW. Type I collagen abrogates the clathrin-mediated internalization of membrane type 1 matrix metalloproteinase (MT1-MMP) via the MT1-MMP hemopexin domain. *J Biol Chem* 2006; **281**: 6826–40.
21 Ogawa M, Kosaka N, Choyke PL, Kobayashi H. H-type dimer formation of fluorophores: a mechanism for activatable, *in vivo* optical molecular imaging. *ACS Chem Biol* 2009; **4**: 535–46.
22 Nakada M, Okada Y, Yamashita J. The role of matrix metalloproteinases in glioma invasion. *Front Biosci* 2003; **8**: e261–9.
23 Yu M, Bowden ET, Sitlani J *et al.* Tyrosine phosphorylation mediates ConA-induced membrane type 1-matrix metalloproteinase expression and matrix metalloproteinase-2 activation in MDA-MB-231 human breast carcinoma cells. *Cancer Res* 1997; **57**: 5028–32.
24 Ueda J, Kajita M, Suenaga N, Fujii K, Seiki M. Sequence-specific silencing of MT1-MMP expression suppresses tumor cell migration and invasion: importance of MT1-MMP as a therapeutic target for invasive tumors. *Oncogene* 2003; **22**: 8716–22.
25 Belien AT, Paganetti PA, Schwab ME. Membrane-type 1 matrix metalloprotease (MT1-MMP) enables invasive migration of glioma cells in central nervous system white matter. *J Cell Biol* 1999; **144**: 373–84.
26 Temma T, Sano K, Kuge Y *et al.* Development of a radiolabeled probe for detecting membrane type-1 matrix metalloproteinase on malignant tumors. *Biol Pharm Bull* 2009; **32**: 1272–7.
27 Wang X, Ma D, Keski-Oja J, Pei D. Co-recycling of MT1-MMP and MT3-MMP through the trans-Golgi network. Identification of DKV582 as a recycling signal. *J Biol Chem* 2004; **279**: 9331–6.
28 Uekita T, Itoh Y, Yana I, Ohno H, Seiki M. Cytoplasmic tail-dependent internalization of membrane-type 1 matrix metalloproteinase is important for its invasion-promoting activity. *J Cell Biol* 2001; **155**: 1345–56.

doi: 10.1111/j.1349-7006.2011.02020.x

29 Remacle A, Murphy G, Roghi C. Membrane type I-matrix metalloproteinase (MT1-MMP) is internalised by two different pathways and is recycled to the cell surface. *J Cell Sci* 2003; **116**: 3905–16.
30 Gálvez BG, Matías-Roman S, Yáñez-Mo M, Vicente-Manzanares M, Sánchez-Madrid F, Arroyo AG. Caveolae are a novel pathway for membrane-type 1 matrix metalloproteinase traffic in human endothelial cells. *Mol Biol Cell* 2004; **15**: 678–87.
31 Weissleder R. A clearer vision for *in vivo* imaging. *Nat Biotechnol* 2001; **19**: 316–7.
32 Matsumura Y, Maeda H. A new concept for macromolecular therapeutics in cancer chemotherapy: mechanism of tumoritropic accumulation of proteins and the antitumor agent smancs. *Cancer Res* 1986; **46**: 6387–92.
33 Maeda H, Seymour LW, Miyamoto Y. Conjugates of anticancer agents and polymers: advantages of macromolecular therapeutics *in vivo*. *Bioconjug Chem* 1992; **3**: 351–62.
34 Watkins GA, Jones EF, Scott Shell M *et al.* Development of an optimized activatable MMP-14 targeted SPECT imaging probe. *Bioorg Med Chem* 2009; **17**: 653–9.
35 Kondo M, Asai T, Katanasaka Y *et al.* Anti-neovascular therapy by liposomal drug targeted to membrane type-1 matrix metalloproteinase. *Int J Cancer* 2004; **108**: 301–6.
36 Packard BZ, Artym VV, Komoriya A, Yamada KM. Direct visualization of protease activity on cells migrating in three-dimensions. *Matrix Biol* 2009; **28**: 3–10.
37 Zhao T, Harada H, Teramura Y *et al.* A novel strategy to tag matrix metalloproteinases-positive cells for *in vivo* imaging of invasive and metastatic activity of tumor cells. *J Control Release* 2010; **144**: 109–14.
38 Sato H, Takino T, Okada Y *et al.* A matrix metalloproteinase expressed on the surface of invasive tumour cells. *Nature* 1994; **370**: 61–5.
39 Frangioni JV. *In vivo* near-infrared fluorescence imaging. *Curr Opin Chem Biol* 2003; **7**: 626–34.
40 Sharma R, Wendt JA, Rasmussen JC, Adams KE, Marshall MV, Sevick-Muraca EM. New horizons for imaging lymphatic function. *Ann N Y Acad Sci* 2008; **1131**: 13–36.
41 Kitai T, Inomoto T, Miwa M, Shikayama T. Fluorescence navigation with indocyanine green for detecting sentinel lymph nodes in breast cancer. *Breast Cancer* 2005; **12**: 211–5.
42 Kikuchi M, Hosokawa K. Near-infrared fluorescence venography: a navigation system for varicose surgery. *Dermatol Surg* 2009; **35**: 1495–8.

Supporting Information

Additional Supporting Information may be found in the online version of this article:

Fig. S1. Western blotting analyses of MT1-MMP expression of C6 cells and MCF-7 cells.

Fig. S2. Fluorescence and bright-field images of organs 48 h after anti-MT1-MMP mAb-ROX administration. The method was the same as that shown in Table 1.

Data S1. Materials and methods.

Please note: Wiley-Blackwell are not responsible for the content or functionality of any supporting materials supplied by the authors. Any queries (other than missing material) should be directed to the corresponding author for the article.

Bioorganic & Medicinal Chemistry 19 (2011) 4312–4321

Contents lists available at ScienceDirect

Bioorganic & Medicinal Chemistry

journal homepage: www.elsevier.com/locate/bmc

Synthesis and evaluation of a radioiodinated trisaccharide derivative as a synthetic substrate for a sensitive *N*-acetylglucosaminyltransferase V radioassay

Takahiro Mukai [a], Masayori Hagimori [b], Kenji Arimitsu [c], Takahiro Katoh [c], Misa Ukon [b], Tetsuya Kajimoto [c], Hiroyuki Kimura [b], Yasuhiro Magata [d], Eiji Miyoshi [e], Naoyuki Taniguchi [f], Manabu Node [c], Hideo Saji [b,*]

[a] Department of Biophysical Chemistry, Kobe Pharmaceutical University, 4-19-1 Motoyamakita-machi, Higashinada-ku, Kobe 658-8558, Japan
[b] Department of Patho-functional Bioanalysis, Graduate School of Pharmaceutical Sciences, Kyoto University, Yoshida Shimoadachi-cho, Sakyo-ku, Kyoto 606-8501, Japan
[c] Department of Pharmaceutical Manufacturing Chemistry, Kyoto Pharmaceutical University, Misasagi Nakauchi-cho, Yamashina-ku, Kyoto 607-8414, Japan
[d] Laboratory of Genome Bio-Photonics, Photon Medical Research Center, Hamamatsu University School of Medicine, 1-20-1 Handayama, Hamamatsu 431-3192, Japan
[e] Department of Molecular Biochemistry & Clinical Investigation, Osaka University Graduate School of Medicine, 1-7 Yamadaoka, Suita 565-0871, Japan
[f] System Glycobiology Research Group Advanced Science Institute, RIKEN 2-1 Hirosawa, Wako 351-0198, Japan

ARTICLE INFO

Article history:
Received 26 March 2011
Revised 21 May 2011
Accepted 23 May 2011
Available online 27 May 2011

Keywords:
N-acetylglucosaminyltransferase V
Radiolabeled substrate
Radioassay

ABSTRACT

N-acetylglucosaminyltransferase V (GnT-V) is one of the most relevant glycosyltransferases to tumor invasion and metastasis. Based on previous findings of molecular recognition between GnT-V and synthetic substrates, we designed and synthesized a *p*-iodophenyl-derivatized trisaccharide, 2-(4-iodophenyl)ethyl 6-*O*-[2-*O*-(2-acetamido-2-deoxy-β-D-glucopyranosyl)-α-D-mannopyranosyl]-β-D-glucopyranoside (IPGMG, **1**) and its radiolabeled form, [^{125}I]IPGMG ([^{125}I]**1**), for use in assays of GnT-V activity *in vitro*. The tributyltin derivative, 2-[4-(*n*-tributylstannyl)phenyl]ethyl 6-*O*-[2-*O*-(3,4,6-tri-*O*-acetyl-2-acetamido-2-deoxy-β-D-glucopyranosyl)-3,4,6-tri-*O*-acetyl-α-D-mannopyranosyl]-2,3,4-tri-*O*-acetyl-β-D-glucopyranoside (**21**), was synthesized as a precursor for the preparation of [^{125}I]**1**. The iododestannylation of **21** using hydrogen peroxide as an oxidant followed by deacetylation yielded [^{125}I]**1**. When [^{125}I]**1** was incubated in GnT-V-expressing cells with a UDP-GlcNAc donor, the production of β1–6GlcNAc-bearing IPGMG (IPGGMG, **2**) was confirmed by radio-HPLC. In kinetic analysis, **1** was found to be a good substrate with a K_m of 23.7 μM and a V_{max} of 159 pmol/h. μg protein. [^{125}I]**1** would therefore be a useful synthetic substrate for the quantitative determination of GnT-V activity.

1. Introduction

The sugar chains of glycoproteins on cell surfaces, which are constructed by glycosyltransferases and glycosidases, change during particular biological events including development, carcinogenesis, and malignant transformation. Numerous studies conducted in the last two decades have demonstrated that *N*-acetylglucosaminyltransferase V (GnT-V) is relevant to tumor invasion and metastasis. Since Cummings first reported its expression in mouse lymphoma cells in 1982,[1] GnT-V has been shown to be highly expressed in various cancer cell lines and tissues from the early stages of tumorigenesis.[2–8] In addition, studies using GnT-V-deficient mice have directly demonstrated an essential role of GnT-V in tumor growth and metastasis.[9,10]

GnT-V catalyzes the transfer of an *N*-acetylglucosamine (GlcNAc) residue from a donor, UDP-GlcNAc, to an acceptor, the mannose α1–6 side chain of the trimannosyl core of *N*-glycans, to form a GlcNAcβ1–6Man linkage. This activity has been assessed predominantly using radiolabeled donors or fluorescent-labeled acceptors. In the former case, the production of sugar chains, the non-reducing ends of which are modified with radiolabeled GlcNAc by the enzymatic reaction, is measured through the use of a UDP-[^{3}H]GlcNAc or UDP-[^{14}C]GlcNAc donor.[2,11,12] However, there is a problem with specificity since UDP-GlcNAc functions as a substrate for many glycosyltransferases. In the latter case, a GnT-specific acceptor, GlcNAcβ1-2Manα1-3-(GlcNAcβ1-2Manα1-6)Manβ1-4GlcNAcβ1-4GlcNAc, is labeled with 2-aminopyridine to yield a fluorescent substrate (Gn,Gn-bi-PA). This acceptor is obtained from the carbohydrate moiety of human transferrin through laborious and time-consuming processes, repeated digestion with various enzymes, chemical modifications, and purification.[13–15] Moreover, the PA-oligosaccharide could still be a substrate of GnT-III.

Thus, we planned and produced a GnT-V-specific radioiodinated substrate for use in assays of GnT-V activity *in vitro*. First, to ensure a high degree of specificity, GlcNAcβ1-2Manα1-6Glc[12,16–18] was

* Corresponding author. Tel.: +81 75 753 4566; fax: +81 75 753 4568.
E-mail address: hsaji@pharm.kyoto-u.ac.jp (H. Saji).

0968-0896/$ - see front matter © 2011 Elsevier Ltd. All rights reserved.
doi:10.1016/j.bmc.2011.05.047

employed as the saccharide moiety on the basis of previous findings; (i) it could not be a substrate of GnT-I and GnT-IV because of the lack of an acceptor site for GnT-I and GnT-IV, that is, a Man residue linked to the bisecting Man with an α1–3 linkage, (ii) it is a poor substrate of GnT-III because of the replacement of the acceptor residue, that is, bisecting Man, with Glc, and (iii) it already carries an GlcNAc residue that should be transferred by GnT-II. Second, the 1-hydroxyl of the reducing terminal Glc, which was adopted as a substitute of the bisecting Man, was conjugated with a hydrophobic phenethyl group without loss of activity.[11,12,16–18] Finally, the radioiodine ^{125}I was considered to be incorporated into the *para*-position of the phenyl ring immediately before the biological assay because the *para*-substitution of iodine is effective in preventing deiodination *in vivo*.[19] The *p*-iodophenyl-derivatized trisaccharide, 2-(4-iodophenyl)ethyl 6-*O*-[2-*O*-(2-acetamido-2-deoxy-β-D-glucopyranosyl)-α-D-mannopyranosyl]-β-D-glucopyranoside, was expected to behave as a substrate for *in vitro* assays of GnT-V activity.

Herein, we report synthesis of an unlabeled IPGMG (**1**), a ^{125}I-labeled IPGMG ([^{125}I]**1**), and the *N*-acetylglucosaminylated product β1-6GlcNAc-bearing IPGMG (IPGGMG, **2**). The reaction kinetics of [^{125}I]**1** were evaluated in GnT-V-expressing cells and its recognition by GnT-V was compared with that of Gn,Gn-bi-PA. From these results, the usefulness of [^{125}I]**1** for the GnT-V assay was assessed (Fig. 1).

2. Results and discussion

2.1. Chemistry

For the synthesis of **1** and [^{125}I]**1**, glycosylation of 3,4,6-tri-*O*-acetyl-2-*O*-(3,4,6-tri-*O*-acetyl-2-acetamido-2-deoxy-β-D-glucopyranosyl)-α-D-mannopyranosyl bromide (**3**) and 2-(4-iodophenyl) ethyl-2,3,4-tri-*O*-acetyl-β-D-glucopyranoside (**4**) was used as a key reaction (Scheme 1).

Synthesis of the bromide **3** began with the condensation, which was promoted by silver trifluoromethanesulfonate and collidine, of benzyl 3-*O*-benzyl-4,6-*O*-benzylidene-α-D-mannopyranoside (**5**)[20] and 3,4,6-tri-*O*-acetyl-2-deoxy-2-phthalimido-β-D-glucopyranosyl bromide (**6**)[21] to afford disaccharide **7** (57%). Subsequent treatment of **7** with hydrazine hydrate followed by acetylation yielded **8** (80%, two steps). Debenzylidenation of **8** in 70% AcOH and subsequent acetylation yielded intermediate **9** (80%, two steps), whose hydrogenolysis and acetylation afforded octaacetate **10** (86%, two steps). Subsequent treatment of **10** with 30% HBr–AcOH afforded **3**, which was used as the glycosyl donor for the next reaction (Scheme 2).

Synthesis of glycosyl acceptor **4** was achieved by the coupling of 2-(4-bromophenyl)ethyl alcohol and 2,3,4-tri-*O*-acetyl-6-*O*-allyloxycarbonyl-α-D-glucopyranosyl trichloroacetimidate (**13**) prepared from 1,2,3,4-tetra-*O*-acetyl-β-D-glucopyranose (**11**)[22] in three steps: protection of the 6-OH group with an allyloxycarbonyl group that afforded **12**, anomerical deacetylation of **12** with piperidine, and reaction with CCl_3CN in the presence of DBU that afforded the imidate **13**. (Scheme 3).

Glycosylation of 2-(4-bromophenyl)ethyl alcohol with imidate **13** led to 2-(4-bromophenyl)ethyl 2,3,4-tri-*O*-acetyl-6-*O*-allyloxycarbonyl-β-D-glucopyranoside (**14**) (72%), which was subjected to palladium-catalyzed deallylation to afford **15** (94%). **15** was reacted with ethyl vinyl ether in the presence of a catalytic amount of pyridinium *p*-toluenesulfonate to form **16** (99%). At this point, replacement of the bromo group with an iodo group was investigated before developing the route to **1** and [^{125}I]**1**. The intermediate, 2-[4-(tributylstannyl)phenyl]ethyl 2,3,4-tri-*O*-acetyl-6-*O*-(1-ethoxyethyl)-β-D-glucopyranoside (**17**), was prepared from **16** using a bromo-to-tributyltin exchange reaction catalyzed by Pd(0) (47%). The tributyltin derivative **17** was readily converted to 2-(4-iodophenyl)ethyl 2,3,4-tri-*O*-acetyl-6-*O*-(1-ethoxyethyl)-β-D-glucopyranoside (**18**) by reaction with iodine (94%). Treatment of **17** and **18** with pyridinium *p*-toluenesulfonate in methanol yielded **19** (95%) and **4** (98%), respectively (Scheme 3).

The treatment of glycosyl donor **3** with glycosyl acceptor **4** in the presence of silver carbonate and silver perchlorate in dichloromethane and toluene yielded **20** (67%), which was deacetylated to furnish the target compound **1** (59%) (Scheme 4). Next, synthesis of the precursor of [^{125}I]**1**, **22**, was attempted from which the tributyltin group was expected to be facilely replaced with a radioactive iodo group by iododestannylation to yield [^{125}I]**1**. However, deacetylation of **21**, which was obtained by the condensation of **3** and **19** in the presence of silver perchlorate and collidine (43%), did not yield **22**. Therefore, the tributyltin derivative **21** was transformed into the fully protected and radiolabeled trisaccharide [^{125}I]**20** by an iododestannylation reaction using hydrogen peroxide as the oxidant. Conventional deacetylation of [^{125}I]**20** afforded the desired radioiodinated compound [^{125}I]**1** (Scheme 4). It was anticipated that no-carrier-added preparation would result in a final product bearing a theoretical specific activity similar to that of ^{125}I. The radiochemical identity of [^{125}I]**1** was verified by co-injection with nonradioactive **1** and comparison of their HPLC profiles. The final radioiodinated compound [^{125}I]**1** showed a single peak of radioactivity at the same retention time as that of nonradioactive **1**. The radioiodinated product was obtained in 50% radiochemical yield with a radiochemical purity of >95% after HPLC.

Finally, 2-(4-iodophenyl)ethyl 6-*O*-[2,6-di-*O*-(2-acetamido-2-deoxy-β-D-glucopyranosyl)-α-D-mannopyranosyl]-β-D-glucopyranoside (IPGGMG, **2**), the *N*-acetylglucosaminylated product of **1**, was synthesized starting with removal of the benzyliden group of **7** with 70% AcOH to afford **23** (83%). Selective silylation of 6-OH of the mannose unit with *tert*-butyldimethylsilyl chloride yielded **24** (94%), the remaining hydroxyl group of which was acetylated to afford **25** (99%). Treatment of **25** with pyridinium *p*-toluenesulfonate afforded **26** (75%), whose glycosylation with the bromide **6**

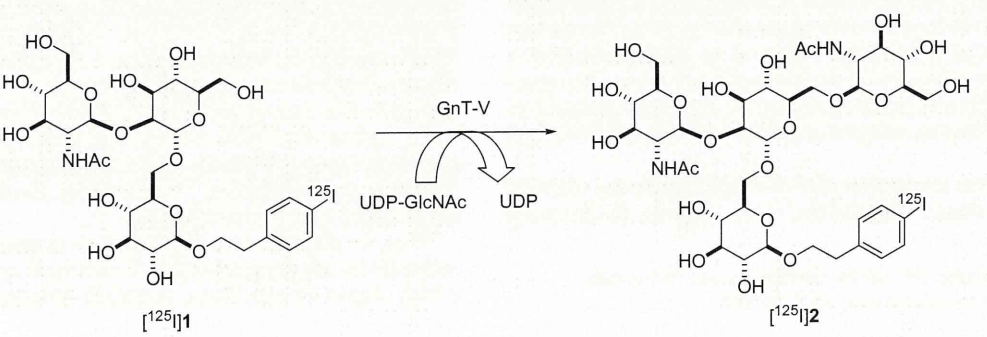

Figure 1. Glycosylation of [^{125}I]**1** by GnT-V.

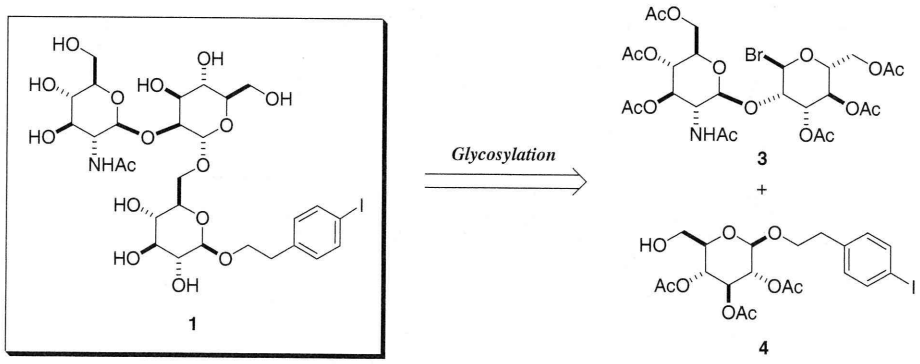

Scheme 1. Synthesis of trisaccharide **1**.

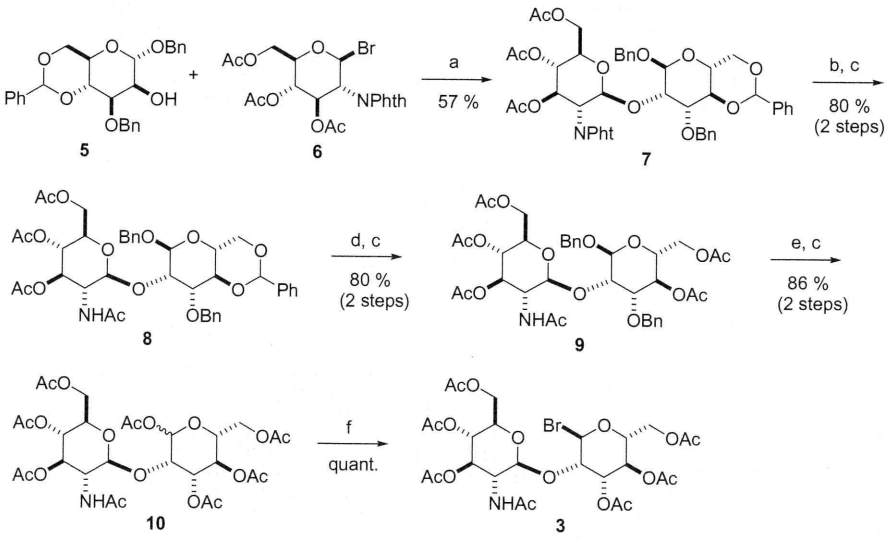

Scheme 2. Synthesis of disaccharide **3**. Reagents and condition: (a) AgOTf, collidine, CH_3NO_2, (b) $NH_2NH_2 \cdot H_2O$, EtOH, (c) Ac_2O, pyridine, (d) 70% AcOH, (e) 10% Pd-C, H_2, EtOH, (f) 30% HBr-AcOH.

promoted by silver trifluoromethanesulfonate and collidine yielded **27** (40%). Removal of the *N*-phthalimido groups with hydrazine hydrate and subsequent acetylation yielded **28** (93%, two steps). Cleavage of the benzyl groups of **28** by hydrogenolysis followed by acetylation yielded **29** (72%, two steps). Treatment of **29** in acetic anhydride with HBr yielded bromide **30**. Glycosylation of **4** with bromide **30** promoted by silver carbonate and silver perchlorate yielded **31** (7%, two steps), which was sequentially deacetylated to furnish the target compound **2** (Scheme 5).

2.2. Biological studies

A typical HPLC profile of the GnT-V-reaction products of [^{125}I]**1** is shown in Figure 2. The reaction products showed peaks at retention times of 21 and 30 min, respectively, identical to those of the nonradioactive compounds **2** and **1**.

This result indicates that GnT-V catalyzes the transfer of a GlcNAc residue from UDP-GlcNAc to [^{125}I]**1** to form a β1–6 linkage, providing evidence that [^{125}I]**1** acts as a substrate for GnT-V.

The kinetics of the conversion of **1** to **2** by GnT-V were determined using the IPGMG solution containing [^{125}I]**1**. This radioiodinated substrate exhibited saturation kinetics at high substrate concentrations (Fig. 3A). The data satisfied the Michaelis–Menten equation, originally developed for enzymatic kinetics. The kinetic parameters were K_m = 23.7 μM and V_{max} = 159 pmol/h·μg protein, determined from the double-reciprocal Lineweaver–Burk plot (Figure 3B). The K_m value is one order of magnitude lower than that for a fluorescent substrate, Gn,Gn-bi-PA.

The novel radioiodinated substrate [^{125}I]**1** was used to assay GnT-V activity in crude extracts of various tissues in normal rats. To compare the findings with previous results obtained using Gn,Gn-bi-PA as a substrate, we assayed the GnT-V activity under similar experimental conditions.[13] The results are summarized in Table 1. This enzyme was uniformly distributed in rat tissues with relatively high activity levels in the small intestine and serum. A similar tendency was observed in a previous investigation using Gn,Gn-bi-PA.[13] The reaction velocity using [^{125}I]**1** was 3- to 22-fold greater than that using Gn,Gn-bi-PA. These findings demonstrate that **1** serves as a better substrate for GnT-V than Gn,Gn-bi-PA.

3. Conclusions

We successfully designed and synthesized a novel radioiodinated trisaccharide derivative, [^{125}I]**1**, as a synthetic substrate for

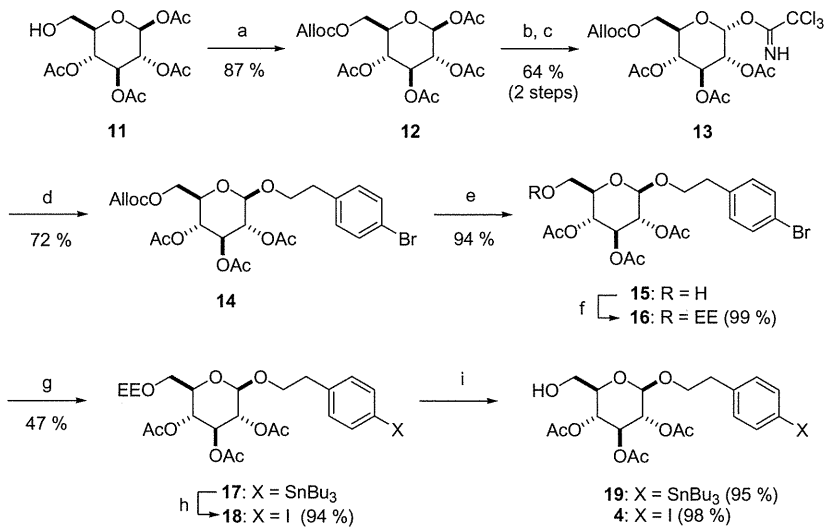

Scheme 3. Synthesis of glucose derivative **4**. Reagents and condition: (a) AllocCl, pyridine, THF, (b) piperidine, THF, (c) CCl_3CN, DBU, CH_2Cl_2, (d) 2-(4-bromophenyl)ethyl alcohol, $BF_3 \cdot Et_2O$, CH_2Cl_2, (e) $Pd(PPh_3)_4$, PPh_3, HCO_2H, THF, (f) ethyl vinyl ether, PPTS, CH_2Cl_2, (g) $Pd(PPh_3)_4$, PPh_3, $(n\text{-}Bu_3Sn)_2$, DMF, (h) I_2, CH_2Cl_2, (i) PPTS, MeOH.

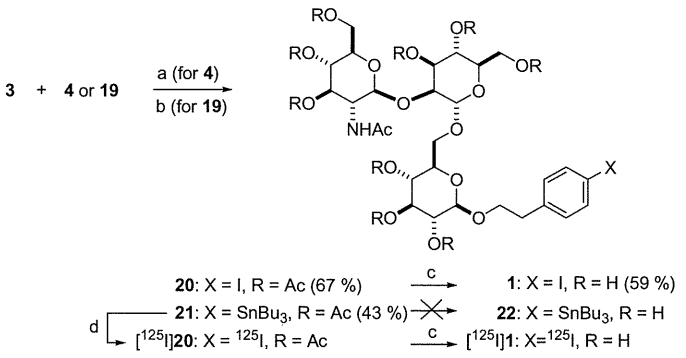

Scheme 4. Synthesis of **1** and [^{125}I]**1**. Reagents and condition: (a) $AgClO_4$, Ag_2CO_3, CH_2Cl_2, toluene, (b) $AgClO_4$, collidine, CH_2Cl_2, toluene, (c) NaOMe, MeOH, (d): [^{125}I]NaI, 5% H_2O_2 aq, 0.1 % HCl aq.

GnT-V. [^{125}I]**1** exhibited higher affinity than a fluorescent substrate, Gn,Gn-bi-PA, suggesting it to be the preferred acceptor for this enzyme. The present findings contribute to the development of sensitive *in vitro* GnT-V assays.

4. Experimental sections

4.1. Synthetic methods

All reagents were commercial products and used without further purification unless otherwise indicated. ^{1}H NMR spectra were obtained on a JEOL JNM EX-270, JNM AL-300, and Varian Unity INOVA 400 spectrometer. Signals are given in ppm using tetramethylsilane as an internal standard. MS spectra were determined on a JEOL JMX-SX102A QQ and Shimadzu LCMS-QP8000α mass spectrometer.

4.1.1. Benzyl 3-*O*-benzyl-4,6-*O*-benzylidiene-2-*O*-[3,4,6-tri-*O*-acetyl-2-deoxy-2-phthalimido-β-D-glucopyranosyl]-α-D-manno pyranoside (7)

To a mixture of **5** (255 mg, 0.57 mmol), silver trifluoromethanesulfonate (263 mg, 1.02 mmol), and collidine (135 μL, 1.02 mmol) in nitromethane (1 mL) was added a nitromethane (2 mL) solution of **6** (426 mg, 0.86 mmol) at −20 °C. The reaction mixture was stirred at −20 °C for 10 min and room temperature for 1.5 h before being filtered through Celite® and concentrated *in vacuo*. The residue was purified by silica gel chromatography (toluene/diethyl ether = 3:1) to afford **7** (280 mg, 57%). ^{1}H NMR (300 MHz, $CDCl_3$) δ: 1.93, 2.08 and 2.09 (each s, 3H), 3.20 (t, J = 10.1 Hz, 1H), 3.52–3.65 (m, 1H), 3.71–3.76 (m, 1H), 3.88–3.96 (m, 3H), 4.15–4.17 (m, 1H), 4.25 (d of ABd, J_{AB} = 12.2 Hz, J = 2.3 Hz, 1H), 4.33 (ABd, J_{AB} = 11.7 Hz, 1H), 4.34 (d of ABd, J_{AB} = 12.2 Hz, J = 4.7 Hz, 1H), 4.52 (ABd, J_{AB} = 11.7 Hz, 1H), 4.53 (dd, J = 10.8 and 8.4 Hz, 1H), 4.64 (s, 1H), 4.67–4.76 (m, 2H), 5.22 (t, J = 9.6 Hz, 1H), 5.44 (d, J = 8.4 Hz, 1H), 5.50 (s, 1H), 5.92 (dd, J = 10.7 and 9.1 Hz, 1H), 7.20–7.48 (m, 15H), 7.77–7.82 (m, 2H), 7.88–7.91 (m, 2H); MS FAB(+) *m/z* 866 [(M+H)$^+$, 26]; HR-MS calcd for $C_{47}H_{47}NO_{15}Na$ [(M+Na)$^+$] 888.2843, found: 888.2845.

4.1.2. Benzyl 3-*O*-benzyl-4,6-*O*-benzylidiene-2-*O*-[3,4,6-tri-*O*-acetyl-2-acetamido-2-deoxy-β-D-glucopyranosyl]-α-D-manno pyranoside (8)

To an ethanol (50 mL) solution of **7** (900 mg, 1.04 mmol) was added hydrazine·hydrate (80% in water, 1.5 mL). The reaction mixture was heated at reflux for 4.5 h before being filtered and concentrated in vacuo. The residue was purified by silica gel chroma

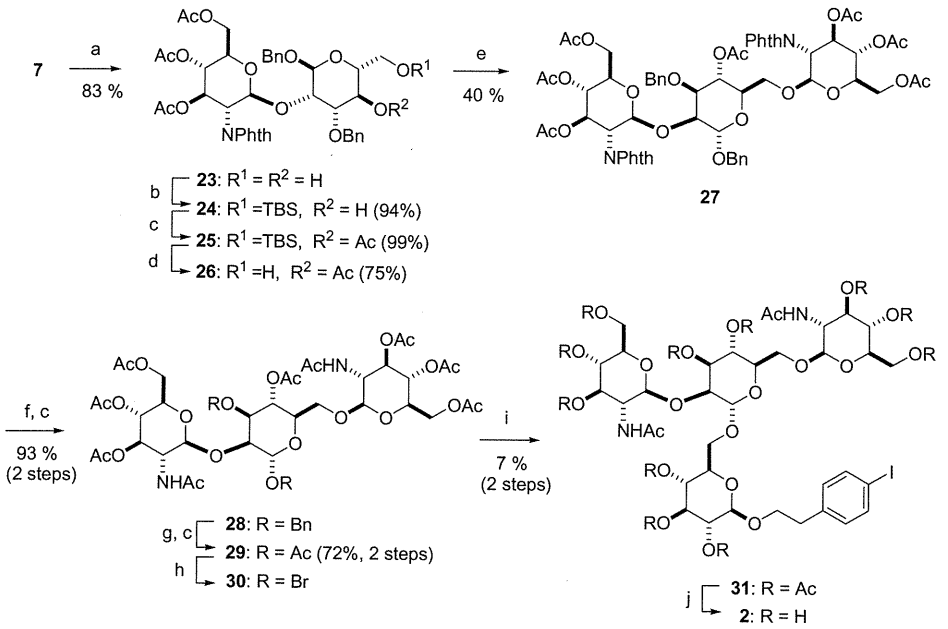

Scheme 5. Synthesis of tetrasaccharide **2**. Reagents and condition: (**a**) 70% AcOH, (**b**) TBSCl, imidazole, DMF, (**c**) Ac_2O, pyridine, (**d**) PPTS, CH_2Cl_2, (**e**) **6**, AgOTf, collidine, CH_3NO_2, (**f**) NH_2NH_2 H2O, EtOH, (**g**) 10% Pd-C, H_2, EtOH, (**h**) 30% HBr-AcOH, Ac_2O, (**i**) **4**, $AgClO_4$, Ag_2CO_3, CH_2Cl_2, toluene, (**j**) NaOMe, MeOH.

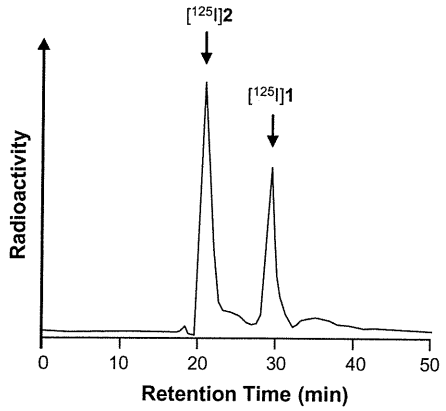

Figure 2. Chromatogram of reaction products of [^{125}I]**1**.

tography (chloroform/methanol = 3:1) to afford the dephthaloyl product (500 mg, 95%). A mixture of the dephthaloyl product (500 mg, 0.82 mmol) and acetic anhydride (2.5 mL) in pyridine (5 mL) was stirred overnight at room temperature. The mixture was poured into ice water, and extracted with ethyl acetate. The organic layer was washed with water, dried over sodium sulfate, filtered, and concentrated in vacuo. The residue was purified by silica gel chromatography (chloroform/methanol = 3:1) to afford **8** (625 mg, 84%). ^{1}H NMR (400 MHz, $CDCl_3$) δ: 1.73, 2.01, 2.02 and 2.02 (each s, 3H) 3.46 (ddd, J = 9.9, 8.3 and 7.6 Hz, 1H), 3.70–3.78 (m, 1H), 3.82–3.86 (m, 2H), 4.01–4.04 (m, 1H), 4.11–4.24 (m, 5H), 4.49 (ABd, J_{AB} = 11.7 Hz, 1H), 4.70 (ABd, J_{AB} = 11.4 Hz, 1H), 4.71 (ABd, J_{AB} = 11.7 Hz, 1H), 4.80 (ABd, J_{AB} = 11.4 Hz, 1H), 4.86 (d, J = 1.6 Hz, 1H), 5.00 (dd, J = 10.1 and 9.3 Hz, 1H), 5.12 (d, J = 8.4 Hz, 1H), 5.52 (d, J = 7.5 Hz, 1H), 5.64 (s, 1H), 5.67 (dd, J = 10.6 and 9.3 Hz, 1H), 7.27–7.40 (m, 13H), 7.49–7.52 (m, 2H); MS FAB(+) m/z 778 [(M+H)$^+$, 5]; HR-MS calcd for $C_{41}H_{48}NO_{14}$ [(M+H)$^+$] 778.3075, found: 778.3070.

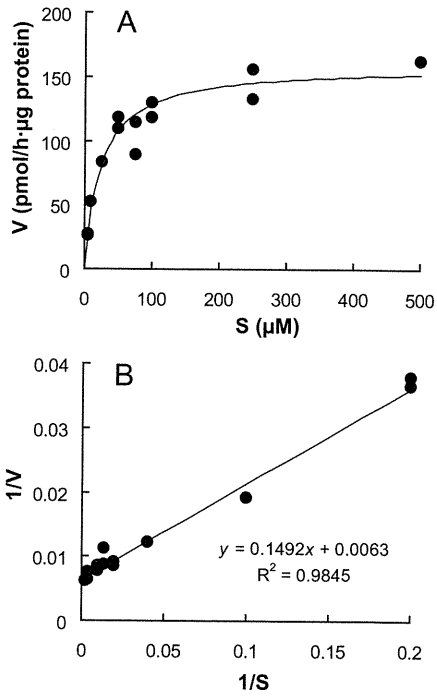

Figure 3. (A) Michaelis–Menten's curve of the GnT-V-catalyzed reaction: (B) Lineweaver–Burk plot of the GnT-V-catalyzed reaction.

4.1.3. Benzyl 4,6-di-*O*-acetyl-3-*O*-benzyl-2-*O*-[3,4,6-tri-*O*-acetyl-2-acetamido-2-deoxy-β-D-glucopyranosyl]-α-D-mannopyrano side (9)

A solution of **8** (160 mg, 0.21 mmol) and 70% acetic acid (2 mL) was heated to 55 °C for 6.5 h. The mixture was poured into ice water, neutralized with sodium hydrogencarbonate,

Table 1
GnT-V activity in rat tissues determined with [^{125}I]**1** or Gn,Gn-bi-PA as a substrate.

Tissue	Activity (pmol/h mg protein)			
	[^{125}I]IPGMG [a]		Gn,Gn-bi-PA [b]	
Heart	31	± 1	10	±1
Liver	48	± 5	8.2	±0.8
Stomach	116	± 65	25	±1
Lung	179	± 6	38	±4
Spleen	244	± 117	21	±2
Brain	261	± 18	38	±1
Kidney	671	± 240	30	±6
Intestine	774	± 67	68	±11
Serum	1284	± 223	112	±53

[a] Each value represents the mean ± SD for three samples.
[b] Results were reported previously.[13]

and extracted with chloroform. The organic layer was washed with a saturated sodium hydrogencarbonate solution, dried over sodium sulfate, filtered, and concentrated in vacuo. The residue was purified by silica gel chromatography (chloroform/methanol = 10:1) to afford the diol compound (125 mg, 91%). A mixture of the diol compound (138 mg, 0.20 mmol) and acetic anhydride (0.5 mL) in pyridine (1 mL) was stirred overnight at room temperature. The mixture was poured into ice water, neutralized with sodium hydrogencarbonate, and extracted with chloroform. The organic layer was washed with water, dried over sodium sulfate, filtered, and concentrated in vacuo. The residue was purified by silica gel chromatography (chloroform/methanol = 20:1) to afford **9** (137 mg, 88%). ^{1}H NMR (400 MHz, $CDCl_3$) δ: 1.82 (s, 3H), 2.00 (s, 6H), 2.01, 2.05 and 2.08 (each s, 3H), 3.29 (ddd, J = 9.9, 8.2 and 7.5 Hz, 1H), 3.71–3.75 (m, 1H), 3.85–3.90 (m, 2H), 4.03 (d of ABd, J_{AB} = 12.1 Hz, J = 2.4 Hz, 1H), 4.10–4.20 (m, 2H), 4.24 (d of ABd, J_{AB} = 12.1 Hz, J = 6.0 Hz, 1H), 4.49 (ABd, J_{AB} = 11.4 Hz, 1H), 4.51 (ABd, J_{AB} = 11.6 Hz, 1H), 4.68 (ABd, J_{AB} = 11.4 Hz, 1H), 4.71 (ABd, J_{AB} = 11.6 Hz, 1H), 4.92 (d, J = 2.0 Hz, 1H), 4.97 (dd, J = 10.1 and 9.2 Hz, 1H), 5.24 (t, J = 9.6 Hz, 1H), 5.27 (d, J = 8.2 Hz, 1H), 5.57 (d, J = 7.1 Hz, 1H), 5.74 (dd, J = 10.5 and 9.2 Hz, 1H), 7.28–7.41 (m, 10H); MS FAB(+) m/z 774 [(M+H)$^+$, 9]; HR-MS calcd for $C_{38}H_{48}NO_{16}$ [(M+H)$^+$] 774.2973, found: 774.2979.

4.1.4. 1,3,4,6-Tetra-*O*-acetyl-2-*O*-(3,4,6-tri-*O*-acetyl-2-acetamido-2-deoxy-β-D-glucopyrosyl)-D-mannopyranose (10)

A mixture of **9** (1.13 g, 1.46 mmol) and Pd-C (10%, *ca.* 600 mg) in a mixed solvent of ethanol (35 mL) and acetic acid (12 mL) was stirred overnight at 50 °C under atmospheric pressure of H_2. The catalysts were filtered, and the filtrate was evaporated. The residue was chromatographed on a silica gel column (chloroform/methanol = 15:2) to give the diol compound (740 mg, quant.). A mixture of the diol compound (225 mg, 0.38 mmol) and acetic anhydride (2 mL) in pyridine (4 mL) was stirred overnight at room temperature. The solvent was removed, and the residue was purified by silica gel chromatography (chloroform/methanol = 10:1) to give **10** (257 mg, 86%). ^{1}H NMR (400 MHz, $CDCl_3$) δ: 1.96, 2.01, 2.02, 2.04, 2.05, 2.08, 2.12 and 2.15 (each s, 3H), 3.28 (ddd, J = 7.1, 5.0 and 2.2 Hz, 1H), 3.87 (ddd, J = 10.6, 8.6 and 8.4 Hz, 1H), 3.96 (ddd, J = 7.3, 4.9 and 2.4 Hz, 1H), 4.02 (d of ABd, J_{AB} = 12.3 Hz, J = 2.2 Hz, 1H), 4.07 (d of ABd, J_{AB} = 12.5 Hz, J = 2.4 Hz, 1H), 4.20 (dd, J = 3.3 and 2.4 Hz, 1H), 4.22 (d of ABd, J_{AB} = 12.5 Hz, J = 5.0 Hz, 1H), 4.25 (d of ABd, J_{AB} = 12.3 Hz, J = 5.0 Hz, 1H), 4.80 (d, J = 8.4 Hz, 1H), 5.04 (dd, J = 10.3 and 3.8 Hz, 1H), 5.06 (dd, J = 10.1 and 1.8 Hz, 1H), 5.33 (dd, J = 10.8 and 4.2 Hz, 1H), 5.36 (dd, J = 10.8 and 4.0 Hz, 1H), 5.79 (d, J = 8.6 Hz, 1H), 5.98 (d, J = 2.0 Hz, 1H); MS FAB(+) *m/z* 678 [(M+H)$^+$, 6]; HR-MS calcd for $C_{28}H_{40}NO_{18}$ [(M+H)$^+$] 678.2245, found: 678.2241.

4.1.5. 3,4,6-Tri-*O*-acetyl-2-*O*-(3,4,6-tri-*O*-acetyl-2-acetamido-2-deoxy-β-D-glucopyrosyl)-α-D-mannopyranosyl bromide (3)

To a solution of **10** (136 mg, 0.20 mmol) and acetic anhydride (1.5 mL) was added hydrogen bromide (30% in acetic acid, 3 mL). The reaction mixture was stirred at room temperature for 4 h under a nitrogen atmosphere, and hydrogen bromide (30% in acetic acid, 3 mL) was added. The mixture was stirred overnight at room temperature, poured into ice water, and extracted with chloroform. The organic layer was washed with water and a saturated sodium hydrogencarbonate solution, dried over sodium sulfate, filtered, and evaporated to give **3** (137 mg, quant.). ^{1}H NMR (400 MHz, $CDCl_3$) δ: 1.95, 2.02, 2.03, 2.05, 2.08, 2.09 and 2.11 (each s, 3H), 3.60 (dt, J = 10.8 and 8.2 Hz, 1H), 3.71–3.77 (m, 1H), 4.00–4.03 (m, 1H), 4.08–4.14 (m, 2H), 4.24–4.28 (m, 2H), 4.48 (dd, J = 3.3 and 1.7 Hz, 1H), 5.01 (dd, J = 9.9 and 9.3 Hz, 1H), 5.08 (d, J = 8.2 Hz, 1H), 5.35–5.52 (m, 3H), 5.87 (d, J = 7.9 Hz, 1H), 6.29 (d, J = 1.3 Hz, 1H); MS FAB(+) *m/z* 698 (M$^+$, 7); HR-MS calcd for $C_{26}H_{36}BrNO_{16}$ (M$^+$) 698.1296, found: 698.1301.

4.1.6. 1,2,3,4-Tetra-*O*-acetyl-6-*O*-allyloxycarbonyl-β-D-glucopyranose (12)

To a tetrahydrofuran (30 mL) solution of 1,2,3,4-tetra-*O*-acetyl-β-D-glucopyranose (**11**) (1.38 g, 4.31 mmol) in an ice bath were added allyl chloroformate (1.37 mL, 12.9 mmol) and pyridine (1.39 mL, 17.2 mmol). The reaction mixture was stirred at room temperature for 2 h under a nitrogen atmosphere, poured into aqueous ammonium chloride (15 mL), and extracted with ethyl acetate. The organic layer was washed with brine, dried over sodium sulfate, filtered, and concentrated in vacuo. The residue was purified by silica gel chromatography (hexane/ethyl acetate = 2:1) to afford **12** (1.63 g, 87%). ^{1}H NMR (300 MHz, $CDCl_3$) δ: 2.01, 2.03, 2.04 and 2.10 (each s, 3H), 3.84 (m, 1H), 4.22–4.32 (m, 2H), 4.61–4.63 (m, 2H), 5.06–5.16 (m, 2H), 5.23–5.39 (m, 3H), 5.74 (d, J = 7.7 Hz, 1H), 5.86–5.99 (m, 1H); MS FAB(+) m/z 455 [(M+Na)$^+$, 100]; HR-MS calcd for $C_{18}H_{24}O_{12}Na$ [(M+Na)$^+$] 455.1166, found: 455.1171.

4.1.7. 2,3,4-Tri-*O*-acetyl-6-*O*-allyloxycarbonyl-α-D-glucopyranosyl trichloroacetimidate (13)

To a tetrahydrofuran (50 mL) solution of **12** (3.45 g, 11.4 mmol) was added piperidine (2.26 mL, 22.8 mmol). The reaction mixture was stirred at room temperature for 20 h under a nitrogen atmosphere. After the reaction was completed, the mixture was diluted with ethyl acetate. The organic layer was washed with 10% hydrochloric acid and brine, dried over sodium sulfate, filtered, and concentrated in vacuo. The residue was purified by silica gel chromatography (hexane/ethyl acetate = 2:1) to give a crude compound (2.41 g). To a solution of the crude compound (2.41 g) in dichloromethane (30 mL) were added trichloroacetonitrile (1.23 mL, 12.3 mmol) and 1,8-diazabicyclo[5.4.0]undec-7-ene (46 μL, 0.31 mmol). The reaction mixture was stirred at room temperature for 2 h. The solvent was removed, and the residue was purified by silica gel chromatography (hexane/ethyl acetate = 3:1) to afford **13** (2.73 g, 64%, 2 steps). ^{1}H NMR (300 MHz, $CDCl_3$) δ: 2.01, 2.04 and 2.06 (each s, 3H), 4.22–4.33 (m, 3H), 4.62 (dt, J = 1.3 and 5.9 Hz, 2H), 5.12 (dd, J = 3.7 and 10.2 Hz, 1H), 5.19 (t, J = 9.6 Hz, 1H), 5.28 (qd, J = 1.3 and 10.5 Hz, 1H), 5.36 (qd, J = 1.5 and 17.2 Hz, 1H), 5.58 (t, J = 9.6 Hz, 1H), 5.92 (ddt, J = 5.9, 10.5 and 17.2 Hz, 1H), 6.57 (d, J = 3.7 Hz, 1H), 8.69 (s, 1H); MS FAB(+) *m/z* 556 [(M+Na)$^+$, 11]; HR-MS calcd for $C_{18}H_{22}O_{11}Cl_3NNa$ [(M+Na)$^+$] 556.0156, found: 556.0152.

4.1.8. 2-(4-Bromophenyl)ethyl 2,3,4-tri-*O*-acetyl-6-*O*-allyloxycarbonyl-β-D-glucopyranoside (14)

To a dichloromethane (20 mL) solution of **13** (904 mg, 1.69 mmol) and 2-(4-bromophenyl)ethyl alcohol (197 μL, 1.41 mmol) was added boron trifluoride diethyl etherate (36 μL,

0.28 mmol). The reaction mixture was stirred at −20 °C for 2 h, and a saturated sodium hydrogencarbonate solution was added. Following extraction with chloroform, the organic phase was dried over sodium sulfate and filtered. The solvent was removed, and the residue was purified by silica gel chromatography (toluene/diethyl ether = 3:1) to afford **14** (584 mg, 72%). ^{1}H NMR (270 MHz, $CDCl_3$) δ: 1.89, 1.99 and 2.03 (each s, 3H), 2.80–2.86 (m, 2H), 3.58–3.75 (m, 2H), 4.06–4.29 (m, 3H), 4.46 (d, J = 7.9 Hz, 1H), 4.62 (dt, J = 1.3 and 5.9 Hz, 2H), 4.93–5.05 (m, 2H), 5.14–5.40 (m, 3H), 5.85–5.99 (m, 1H), 7.04–7.08 (m, 2H), 7.37–7.40 (m, 2H); MS FAB(+) m/z 595 [(M+Na)$^+$, 54]; HR-MS calcd for $C_{24}H_{29}O_{11}BrNa$ [(M+Na)$^+$] 595.0791, found: 595.0787.

4.1.9. 2-(4-Bromophenyl)ethyl 2,3,4-tri-*O*-acetyl-β-D-glucopyranoside (15)

To a tetrahydrofuran (30 mL) solution of **14** (2.12 g, 3.70 mmol) were added tetrakis(triphenylphosphine)palladium (0) (214 mg, 0.18 mmol), triphenylphosphine (291 mg, 1.11 mmol), and formic acid (279 mL, 7.39 mmol). The reaction mixture was stirred at room temperature for 6 h under a nitrogen atmosphere. After the reaction was completed, the mixture was diluted with ethyl acetate. The organic layer was washed with water and brine, dried over sodium sulfate, filtered, and concentrated in vacuo. The residue was purified by silica gel chromatography (hexane/ethyl acetate = 1:1) to afford **15** (1.70 g, 94%). ^{1}H NMR (300 MHz, $CDCl_3$) δ: 1.89, 2.00 and 2.05 (each s, 3H), 2.81–2.86 (m, 2H), 3.46–3.52 (m, 2H), 3.55–3.67 (m, 3H), 3.71–3.75 (m, 1H), 4.13 (ddd, J = 9.5, 6.1 and 5.9 Hz, 1H), 4.49 (d, J = 7.9 Hz, 1H), 4.96 (dd, J = 9.7 and 7.9 Hz, 1H), 5.01 (dd, J = 9.7 and 9.5 Hz, 1H), 5.21 (t, J = 9.5 Hz, 1H), 7.05–7.08 (m, 2H), 7.38–7.41 (m, 2H); MS FAB(+) m/z 511 [(M+Na)$^+$, 99]; HR-MS calcd for $C_{20}H_{25}O_9BrNa$ [(M+Na)$^+$] 511.0580, found: 511.0573.

4.1.10. 2-(4-Bromophenyl)ethyl 2,3,4-tri-*O*-acetyl-6-*O*-(1-ethoxyethyl)-β-D-glucopyranoside (16)

To a dichloromethane (3 mL) solution of **15** (173 mg, 0.35 mmol) were added ethyl vinyl ether (51 μL, 0.53 mmol), and pyridinium p-toluenesulfonate (9 mg, 0.035 mmol). The reaction mixture was stirred at room temperature for 1 h under a nitrogen atmosphere. The solvent was removed, and the residue was purified by silica gel chromatography (hexane/ethyl acetate = 2:1) to afford **16** (197 mg, 99%). ^{1}H NMR (300 MHz, $CDCl_3$) δ: 1.17 (t, J = 7.1 Hz, 1.5H), 1.18 (t, J = 7.1 Hz, 1.5H), 1.28 (d, J = 5.3 Hz, 1.5H), 1.29 (d, J = 5.3 Hz, 1.5H), 1.89 (s, 1.5H), 1.89 (s, 1.5H), 1.99 (s, 3H), 2.02 (s, 3H), 2.80–2.85 (m, 2H), 3.40–3.70 (m, 6H), 4.06–4.16 (m, 1H), 4.46 (d, J = 7.9 Hz, 1H), 4.70 (q, J = 5.3 Hz, 0.5H), 4.72 (q, J = 5.3 Hz, 0.5H), 4.96 (dd, J = 9.7 and 7.9 Hz, 1H), 5.03 (dd, J = 9.7 and 9.5 Hz, 1H), 5.16 (t, J = 9.5 Hz, 1H), 7.05–7.07 (m, 2H), 7.37–7.40 (m, 2H); MS FAB(+) m/z 583 [(M+Na)$^+$, 34]; HR-MS calcd for $C_{24}H_{33}O_{10}BrNa$ [(M+Na)$^+$] 583.1155, found: 583.1151.

4.1.11. 2-[4-(Tributylstannyl)phenyl]ethyl 2,3,4-tri-*O*-acetyl-6-*O*-(1-ethoxyethyl)-β-D-glucopyranoside (17)

To a N,N-dimethylformamide (5 mL) solution of **16** (161 mg, 0.29 mmol) were added tetrakis(triphenylphosphine)palladium (0) (33 mg, 0.029 mmol), triphenylphosphine (15 mg, 0.057 mmol), and bis(tributyltin) (289 μL, 0.57 mmol). The reaction mixture was stirred at 100 °C for 4 h under a nitrogen atmosphere. The solvent was removed, and the residue was purified by silica gel chromatography (hexane/ethyl acetate = 5:1 to 2:1) to afford **17** (103 mg, 47%). ^{1}H NMR (300 MHz, $CDCl_3$) δ: 0.88 (t, J = 7.3 Hz, 9H), 1.02 (t, J = 8.1 Hz, 6H), 1.17 (t, J = 7.2 Hz, 1.5H), 1.18 (t, J = 7.2 Hz, 1.5H), 1.27–1.36 (m, 9H), 1.47–1.57 (m, 6H), 1.89 (s, 3H), 1.99 (s, 3H), 2.02 (s, 3H), 2.86 (t, J = 6.8 Hz, 2H), 3.43–3.71 (m, 6H), 4.08–4.15 (m, 1H), 4.48 (d, J = 8.1 Hz, 1H), 4.70–4.72 (m, 1H), 4.98 (t, J = 8.1 Hz, 1H), 5.04 (t, J = 9.5 Hz, 1H), 5.17 (t, J = 9.5 Hz, 1H), 7.13–7.16 (m, 2H), 7.35–7.37 (m, 2H); MS FAB(+) m/z 795 [(M+Na)$^+$, 43]; HR-MS calcd for $C_{36}H_{60}O_{10}SnNa$ [(M+Na)$^+$] 795.3106, found: 795.3111.

4.1.12. 2-(4-Iodophenyl)ethyl 2,3,4-tri-*O*-acetyl-6-*O*-(1-ethoxyethyl)-β-D-glucopyranoside (18)

To a dichloromethane (10 mL) solution of **17** (305 mg, 0.40 mmol) was added iodine (201 mg, 0.79 mmol). The reaction mixture was stirred at 0 °C for 2 h under a nitrogen atmosphere, and a saturated sodium hydrogencarbonate and sodium thiosulfate solution was added. Following extraction with chloroform, the organic phase was dried over sodium sulfate and filtered. The solvent was removed, and the residue was purified by silica gel chromatography (toluene/diethyl ether = 3:1) to afford **18** (226 mg, 94%). ^{1}H NMR (300 MHz, $CDCl_3$) δ: 1.17 (t, J = 7.0 Hz, 1.5H), 1.17 (t, J = 7.0 Hz, 1.5H), 1.27 (d, J = 5.5 Hz, 1.5H), 1.29 (d, J = 5.1 Hz, 1.5H), 1.89 (s, 3H), 1.99 (s, 3H), 2.01 (s, 3H), 2.79–2.84 (m, 2H), 3.42–3.69 (m, 6H), 4.10 (dt, J = 9.5 and 5.9 Hz, 1H), 4.45 (d, J = 7.7 Hz, 1H), 4.70 (q, J = 5.1 Hz, 0.5H), 4.71 (q, J = 5.1 Hz, 0.5H), 4.95 (dd, J = 9.7 and 7.7 Hz, 1H), 5.03 (dd, J = 9.7 and 9.5 Hz, 1H), 5.16 (t, J = 9.5 Hz, 1H), 6.92–6.95 (m, 2H), 7.57–7.59 (m, 2H); MS FAB(+) m/z 631 [(M+Na)$^+$, 16]; HR-MS calcd for $C_{24}H_{33}O_{10}INa$ [(M+Na)$^+$] 631.1016, found: 631.1011.

4.1.13. 2-[4-(Tributylstannyl)phenyl]ethyl 2,3,4-tri-*O*-acetyl-β-D-glucopyranoside (19)

A mixture of **17** (310 mg, 0.40 mmol), pyridinium p-toluenesulfonate (10 mg, 0.040 mmol), and methanol (10 mL) was stirred at room temperature for 2 h. The solvent was removed, and the residue was purified by silica gel chromatography (hexane/ethyl acetate = 3:1 to 2:1) to afford **19** (268 mg, 95%). ^{1}H NMR (300 MHz, $CDCl_3$) δ: 0.88 (t, J = 7.2 Hz, 9H), 1.02 (t, J = 8.1 Hz, 6H), 1.33 (sextet, J = 7.2 Hz, 6H), 1.53 (tt, J = 8.1 and 7.2 Hz, 6H), 1.89 (s, 3H), 2.00 (s, 3H), 2.04 (s, 3H), 2.12 (t, J = 6.1 Hz, 1H), 2.86 (dd, J = 7.2 and 6.6 Hz, 2H), 3.46–3.52 (m, 1H), 3.55–3.61 (m, 1H), 3.63–3.76 (m, 2H), 4.13 (dt, J = 9.5 and 6.1 Hz, 1H), 4.53 (d, J = 8.1 Hz, 1H), 4.98 (dd, J = 9.7 and 8.1 Hz, 1H), 5.02 (dd, J = 9.7 and 9.5 Hz, 1H), 5.22 (t, J = 9.5 Hz, 1H), 7.14–7.16 (m, 2H), 7.35–7.38 (m, 2H); MS FAB(+) m/z 723 [(M+Na)$^+$, 100]; HR-MS calcd for $C_{32}H_{52}O_9NaSn$ [(M+Na)$^+$] 723.2531, found: 723.2533.

4.1.14. 2-(4-Iodophenyl)ethyl 2,3,4-tri-*O*-acetyl-β-D-glucopyranoside (4)

To a methanol (10 mL) solution of **18** (222 mg, 0.41 mmol) was added pyridinium p-toluenesulfonate (10 mg, 0.036 mmol). The reaction mixture was stirred at 55 °C for 2 h. The solvent was removed, and the residue was purified by silica gel chromatography (hexane/ethyl acetate = 1:1) to afford **4** (192 mg, 98%). ^{1}H NMR (300 MHz, $CDCl_3$) δ: 1.89, 2.00 and 2.05 (each s, 3H), 2.20 (br.t, J = Hz, 1H), 2.80–2.84 (m, 2H), 3.46–3.52 (m, 1H), 3.55–3.77 (m, 3H), 4.12 (dt, J = 9.5 and 5.9 Hz, 1H), 4.49 (d, J = 7.7 Hz, 1H), 4.96 (dd, J = 9.5 and 7.7 Hz, 1H), 5.01 (t, J = 9.5 Hz, 1H), 5.21 (t, J = 9.5 Hz, 1H), 6.93–6.95 (m, 2H), 7.58–7.60 (m, 2H); MS FAB(+) m/z 559 [(M+Na)$^+$, 100]; HR-MS calcd for $C_{20}H_{25}O_9NaI$ [(M+Na)$^+$] 559.0441, found: 559.0447.

4.1.15. 2-(4-Iodophenyl)ethyl 6-*O*-[2-*O*-(3,4,6-tri-*O*-acetyl-2-acetamido-2-deoxy-β-D-glucopyranosyl)-3,4,6-tri-*O*-acetyl-α-D-mannopyranosyl]-2,3,4-tri-*O*-acetyl-β-D-glucopyranoside (20)

To a solution of **4** (214 mg, 0.40 mmol), dichloromethane (10 mL), and toluene (10 mL) was added silver carbonate (121 mg, 0.44 mmol). The reaction mixture was stirred at room temperature for 1 h under a nitrogen atmosphere, and silver perchlorate (12 mg, 0.060 mmol) was added. After stirring for 20 min at room temperature, a solution of **3** (334 mg, 0.48 mmol), dichloromethane (10 mL), and toluene (10 mL) was added and the mixture was stirred

for another 15 h. After the reaction was completed, the mixture was filtered. The filtrate was concentrated in vacuo, and the residue was purified by silica gel chromatography (hexane/ethyl acetate = 4:1 to ethyl acetate only) to afford **20** (310 mg, 67%). ^{1}H NMR (300 MHz, $CDCl_3$) δ: 1.87, 1.93, 1.94, 2.00, 2.01, 2.01, 2.03, 2.05, 2.09 and 2.09 (each s, 3H), 2.82–2.88 (m, 2H), 3.36–3.45 (m, 1H), 3.51–3.54 (m, 1H), 3.61–3.78 (m, 4H), 3.87–3.92 (m, 1H), 4.00–4.09 (m, 2H), 4.13–4.20 (m, 3H), 4.26–4.32 (m, 1H), 4.47 (d, J = 7.7 Hz, 1H), 4.70 (s, 1H), 4.89–5.05 (m, 4H), 5.08 (d, J = 8.1 Hz, 1H), 5.18 (t, J = 9.5 Hz, 1H), 5.21 (t, J = 9.9 Hz, 1H), 5.60 (t, J = 9.2 Hz, 1H), 5.61 (d, J = 9.2 Hz, 1H), 6.94–6.97 (m, 2H), 7.56–7.59 (m, 2H); MS FAB(+) m/z 1154 [(M+H)$^+$, 3]; HR-MS calcd for $C_{46}H_{61}O_{25}NI$ [(M+H)$^+$] 1154.2578, found: 1154.2588.

4.1.16. 2-[4-(Tributylstannyl)phenyl]ethyl 6-*O*-[2-*O*-(3,4,6-tri-*O*-acetyl-2-acetamido-2-deoxy-β-D-glucopyranosyl)-3,4,6-tri-*O*-acetyl-α-D-mannopyranosyl]-2,3,4-tri-*O*-acetyl-β-D-glucopyranoside (21)

To a solution of **19** (30 mg, 0.043 mmol), dichloromethane (1 mL), and toluene (1 mL) was added collidine (14 μL, 0.10 mmol). The reaction mixture was stirred at room temperature for 20 min under a nitrogen atmosphere, and silver perchlorate (11 mg, 0.052 mmol) was added. After stirring for 20 min at room temperature, a solution of **3** (36 mg, 0.052 mmol), dichloromethane (2 mL), and toluene (2 mL) was added and the mixture was stirred for another 5 h. After the reaction was completed, the mixture was filtered. The filtrate was washed with 1% hydrochloric acid, dried over sodium sulfate, filtered, and concentrated in vacuo. The residue was purified by silica gel chromatography (ethyl acetate) to afford **21** (24 mg, 43%). ^{1}H NMR (300 MHz, $CDCl_3$) δ: 0.88 (t, J = 7.3 Hz, 9H), 1.01 (t, J = 8.2 Hz, 6H), 1.32 (sextet, J = 7.3 Hz, 6H), 1.52 (tt, J = 8.2 and 7.3 Hz, 6H), 1.85 (s, 3H), 1.90 (s, 3H), 1.93 (s, 3H), 2.00 (s, 3H), 2.00 (s, 3H), 2.01 (s, 3H), 2.03 (s, 3H), 2.05 (s, 3H), 2.09 (s, 3H), 2.09 (s, 3H), 2.85–2.91 (m, 2H), 3.38–3.48 (m, 1H), 3.52–3.55 (m, 1H), 3.66–3.80 (m, 4H), 3.90–3.95 (m, 1H), 4.00–4.04 (m, 2H), 4.13–4.21 (m, 3H), 4.26–4.32 (m, 1H), 4.49 (d, J = 7.9 Hz, 1H), 4.69 (s, 1H), 4.91–5.07 (m, 5H), 5.16–5.25 (m, 2H), 5.51–5.62 (m, 2H), 7.13–7.16 (m, 2H), 7.33–7.36 (m, 2H); MS FAB(+) m/z 1318 [(M+H)$^+$, 18]; HR-MS calcd for $C_{58}H_{88}O_{25}NSn$ [(M+H)$^+$] 1318.4668, found: 1318.4672.

4.1.17. 2-(4-Iodophenyl)ethyl 6-*O*-[2-*O*-(2-acetamido-2-deoxy-β-D-glucopyranosyl)-α-D-mannopyranosyl]-β-D-glucopyranoside (1)

To a methanol (10 mL) solution of **20** (188 mg, 0.16 mmol) was added sodium methoxide (28% in methanol, 332 μL, 1.63 mmol) and the mixture was stirred at room temperature for 2 h. After the reaction was completed, the mixture was neutralized with Amberlyst® 15 (ca. 1.0 g) and filtered. The filtrate was concentrated in vacuo and the residue was purified by a recycle HPLC (LC-908, Japan Analytical Industry Co. Ltd. Tokyo, Japan) on a reversed phase column (methanol/distilled water = 7:3) to afford **1** (74 mg, 59%). ^{1}H NMR (300 MHz, CD_3OD) δ: 1.99 (s, 3H), 2.89–2.92 (m, 2H), 3.16–4.04 (m, 21H), 4.28 (d, J = 7.3 Hz, 1H), 4.46 (d, J = 7.7 Hz,1H), 7.06–7.09 (m, 2H), 7.59–7.62 (m, 2H); MS FAB(+) m/z 776 [(M+H)$^+$, 10]; HR-MS calcd for $C_{28}H_{43}O_{16}NI$ [(M+H)$^+$] 776.1627, found: 776.1635.

4.1.18. Benzyl 3-*O*-benzyl-2-*O*-[3,4,6-tri-*O*-acetyl-2-deoxy-2-phthalimido-β-D-glucopyranosyl]-α-D-mannopyranoside (23)

A mixture of **7** (1.45 g, 1.67 mmol) and 70% acetic acid (10 mL) was stirred at 55 °C for 2 h. The mixture was poured into ice water, neutralized with sodium hydrogencarbonate, and extracted with chloroform. The organic layer was washed with a saturated sodium hydrogencarbonate solution, dried over sodium sulfate, filtered, and concentrated in vacuo. The residue was purified by silica gel chromatography (chloroform/methanol = 20:1) to afford **23** (1.07 g, 83%). ^{1}H NMR (300 MHz, $CDCl_3$) δ: 1.26 (br.t, J = 6.6 Hz, 1H), 1.89 (s, 3H), 2.01 (s, 3H), 2.04 (s, 3H), 2.28 (br.s, 1H), 3.12–3.16 (m, 1H), 3.37–3.46 (m, 2H), 3.68–3.69 (m, 2H), 3.84–3.90 (m, 1H), 4.13 (br.s, 1H), 4.20 (d of ABd, J_{AB} = 12.4 Hz, J = 2.4 Hz, 1H), 4.27 (d of ABd, J_{AB} = 12.4 Hz, J = 4.8 Hz, 1H), 4.30 (ABd, J_{AB} = 11.7 Hz, 1H), 4.38 (ABd, J_{AB} = 11.0 Hz, 1H), 4.41 (dd, J = 10.6 and 8.4 Hz, 1H), 4.49 (ABd, J_{AB} = 11.7 Hz, 1H), 4.62 (d, J = 1.5 Hz, 1H), 4.75 (ABd, J_{AB} = 11.0 Hz, 1H), 5.17 (t, J = 9.5 Hz, 1H), 5.36 (d, J = 8.4 Hz, 1H), 5.87 (dd, J = 11.0 and 9.2 Hz, 1H), 7.18–7.21 (m, 2H), 7.28–7.34 (m, 8H), 7.76–7.80 (m, 2H), 7.85–7.88 (m, 2H); MS FAB(+) m/z 800 [(M+Na)$^+$, 53]; HR-MS calcd for $C_{40}H_{43}O_{15}NNa$ [(M+Na)$^+$] 800.2530, found: 800.2527.

4.1.19. Benzyl 3-*O*-benzyl-6-*O*-*tert*-butyldimethylsilyl-2-*O*-[3,4,6-tri-*O*-acetyl-2-deoxy-2-phthalimido-β-D-glucopyranosyl]-α-D-mannopyranoside (24)

To a *N*,*N*-dimethylformamide (10 mL) solution of **23** (1.07 g, 1.38 mmol) were added *tert*-butyldimethylsilyl chloride (311 mg, 2.06 mmol) and imidazole (281 mg, 4.13 mmol). The reaction mixture was stirred at room temperature for 16 h under a nitrogen atmosphere, poured into aqueous ammonium chloride (20 mL), and extracted with ethyl acetate. The organic layer was washed with water, dried over sodium sulfate, filtered, and concentrated in vacuo. The residue was purified by silica gel chromatography (hexane/ethyl acetate = 2:1) to afford **24** (1.15 g, 94%). ^{1}H NMR (300 MHz, $CDCl_3$) δ: -0.13 (s, 3H), -0.12 (s, 3H), 0.78 (s, 9H), 1.86 (s, 3H), 2.00 (s, 3H), 2.03 (s, 3H), 2.64 (br.s, 1H), 3.14–3.20 (m, 1H), 3.41–3.49 (m, 2H), 3.60–3.71 (m, 2H), 3.82–3.87 (m, 1H), 4.13–4.26 (m, 3H), 4.31 (ABd, J_{AB} = 11.4 Hz, 1H), 4.40 (d, J = 9.5 Hz, 1H), 4.45 (ABd, J_{AB} = 11.2 Hz, 1H), 4.56 (ABd, J_{AB} = 11.4 Hz, 1H), 4.64 (s, 1H), 4.78 (ABd, J_{AB} = 11.2 Hz, 1H), 5.16 (t, J = 9.7 Hz, 1H), 5.44 (d, J = 8.1 Hz, 1H), 5.78 (dd, J = 10.6 and 9.2 Hz, 1H), 7.21–7.38 (m, 10H), 7.71–7.74 (m, 2H), 7.82–7.84 (m, 2H); MS FAB(+) m/z 914 [(M+Na)$^+$, 62]; HR-MS calcd for $C_{46}H_{57}O_{15}NSiNa$ [(M+Na)$^+$] 914.3395, found: 914.3398.

4.1.20. Benzyl 4-*O*-acetyl-3-*O*-benzyl-6-*O*-*tert*-butyldimethylsilyl-2-*O*-[3,4,6-tri-*O*-acetyl-2-deoxy-2-phthalimido-β-D-glucopyranosyl]-α-D-mannopyranoside (25)

A mixture of **24** (1.14 g, 1.28 mmol) and acetic anhydride (5 mL) in pyridine (5 mL) was stirred at room temperature for 2 h and methanol (20 mL) was added. The solvent was removed, and the residue was purified by silica gel chromatography (hexane/ethyl acetate = 2:1) to give **25** (1.18 g, 99%). ^{1}H NMR (300 MHz, $CDCl_3$) δ: -0.19 (s, 3H), -0.18 (s, 3H), 0.77 (s, 9H), 1.85 (s, 3H), 1.95 (s, 3H), 2.01 (s, 6H), 3.22 (d of ABd, J_{AB} = 11.3 Hz, J = 7.2 Hz, 1H), 3.40 (d of ABd, J_{AB} = 11.3 Hz, J = 2.6 Hz, 1H), 3.55–3.62 (m, 1H), 3.75–3.81 (m, 2H), 4.11–4.24 (m, 3H), 4.32 (ABd, J_{AB} = 11.6 Hz, 1H), 4.44 (ABd, J_{AB} = 11.7 Hz, 1H), 4.44 (dd, J = 10.8 and 8.6 Hz, 1H), 4.60 (ABd, J_{AB} = 11.6 Hz, 1H), 4.69 (d, J = 2.4 Hz, 1H), 4.70 (ABd, J_{AB} = 11.7 Hz, 1H), 4.88 (t, J = 9.1 Hz, 1H), 5.15 (t, J = 9.5 Hz, 1H), 5.53 (d, J = 8.4 Hz, 1H), 5.74 (dd, J = 10.7 and 9.1 Hz, 1H), 7.22–7.35 (m, 10H), 7.68–7.71 (m, 2H), 7.80–7.83 (m, 2H); MS FAB(+) m/z 956 [(M+Na)$^+$, 45]; HR-MS calcd for $C_{48}H_{59}O_{16}NSiNa$ [(M+Na)$^+$] 956.3501, found: 956.3503.

4.1.21. Benzyl 4-*O*-acetyl-3-*O*-benzyl-2-*O*-[3,4,6-tri-*O*-acetyl-2-deoxy-2-phthalimido-β-D-glucopyranosyl]-α-D-mannopyranoside (26)

A mixture of **25** (1.17 g, 1.25 mmol), pyridinium *p*-toluenesulfonate (32 mg, 0.13 mmol), and methanol (10 mL) was stirred at 50 °C for 2 h. The solvent was removed, and the residue was purified by silica gel chromatography (hexane/ethyl acetate = 1:1) to

afford **26** (765 mg, 75%). ^{1}H NMR (300 MHz, $CDCl_3$) δ: 1.44 (br.dd, J = 9.4 and 4.4 Hz, 1H), 1.88(s, 3H), 1.95 (s, 3H), 2.03 (s, 3H), 2.04 (s, 3H), 3.03–3.10 (m, 1H), 3.17–3.25 (m, 1H), 3.39–3.46 (m, 1H), 3.80–3.84 (m, 2H), 4.10–4.11 (m, 1H), 4.16–4.21 (m, 1H), 4.22–4.28 (m, 1H), 4.35 (ABd, J_{AB} = 11.7 Hz, 1H), 4.42–4.48 (m, 1H), 4.47 (ABd, J_{AB} = 11.9 Hz, 1H), 4.51 (ABd, J_{AB} = 11.7 Hz, 1H), 4.68 (ABd, J_{AB} = 11.9 Hz, 1H), 4.71 (d, J = 2.0 Hz, 1H), 4.93 (t, J = 9.6 Hz, 1H), 5.17 (t, J = 9.6 Hz, 1H), 5.45 (d, J = 8.4 Hz, 1H), 5.82 (dd, J = 10.7 and 9.1 Hz, 1H), 7.17–7.21 (m, 2H), 7.26–7.35 (m, 8H), 7.71–7.74 (m, 2H), 7.83–7.86 (m, 2H); MS FAB(+) *m/z* 842 [(M+Na)$^+$, 100]; HR-MS calcd for $C_{42}H_{45}O_{16}NNa$ [(M+Na)$^+$] 842.2636, found: 842.2639.

4.1.22. Benzyl 2,6-di-*O*-[3,4,6-tri-*O*-acetyl-2-deoxy-2-phthalimido-β-D-glucopyranosyl]-4-*O*-acetyl-3-*O*-benzyl-α-D-mannopyranoside (27)

To a mixture of **26** (564 mg, 0.69 mmol), silver trifluoromethanesulfonate (318 mg, 1.24 mmol), and collidine (164 μL, 1.24 mmol) in nitromethane (5 mL) was added a nitromethane (5 mL) solution of **6** (514 mg, 1.03 mmol) at −20 °C. The reaction mixture was stirred at −20 °C for 30 min and room temperature for 2 h before being filtered through Celite® and concentrated in vacuo. The residue was purified by silica gel chromatography (1st; hexane/ethyl acetate = 1:1, 2nd; chloroform/methanol = 20:1) to afford **27** (337 mg, 40%). ^{1}H NMR (300 MHz, $CDCl_3$) δ: 1.83, 1.86, 1.91, 2.00, 2.01, 2.03 and 2.07 (each s, 3H), 2.87–2.94 (m, 1H), 3.55–3.74 (m, 6H), 4.00–4.01 (m, 1H), 4.07–4.41 (m, 7H), 4.35 (ABd, J_{AB} = 12.0 Hz, 1H), 4.47 (d, J = 2.0 Hz, 1H), 4.59 (ABd, J_{AB} = 12.0 Hz, 1H), 4.73 (t, J = 9.4 Hz, 1H), 5.00 (d, J = 8.3 Hz, 1H), 5.06 (t, J = 9.4 Hz, 1H), 5.12 (t, J = 9.4 Hz, 1H), 5.42 (d, J = 8.6 Hz, 1H), 5.71 (dd, J = 10.7 and 9.1 Hz, 1H), 7.01–7.04 (m, 2H), 7.18–7.29 (m, 8H), 7.61–7.76 (m, 6H), 7.83–7.86 (m, 2H); MS FAB(+) *m/z* 1259 [(M+Na)$^+$, 20]; HR-MS calcd for $C_{62}H_{64}N_2O_{25}Na$ [(M+Na)$^+$] 1259.3696, found: 1259.3704.

4.1.23. Benzyl 2,6-di-*O*-[3,4,6-tri-*O*-acetyl-2-acetamido-2-deoxy-β-D-glucopyranosyl]-4-*O*-acetyl-3-*O*-benzyl-α-D-mannopyranoside (28)

To an ethanol (10 mL) solution of **27** (157 mg, 0.13 mmol) was added hydrazine·hydrate (80% in water, 200 μL). The reaction mixture was heated at reflux for 4 h before being concentrated in vacuo. The residue was dissolved in pyridine (2 mL) and acetic anhydride (2 mL) was added. The mixture was stirred overnight at room temperature and methanol (20 mL) was added. The solvent was removed, and the residue was purified by silica gel chromatography (chloroform/methanol = 20:1) to give **28** (125 mg, 93%, 2 steps). ^{1}H NMR (300 MHz, $CDCl_3$) δ: 1.94, 1.98, 2.02, 2.02, 2.04 and 2.06 (each s, 3H), 2.07 (s, 6H), 2.07 (s, 3H), 2.98 (br dt, J = 7.1 and 9.5 Hz, 1H), 3.13 (br d, J = 10.6 Hz, 1H), 3.56 (br d, J = 9.8 Hz, 1H), 3.64 (ddd, J = 2.6, 4.7 and 9.5 Hz, 1H), 3.79 (br dt, J = 3.0 and 10.1 Hz, 1H), 3.87 (dd, J = 3.7 and 9.8 Hz, 1H), 4.09–4.15 (m, 5H), 4.21–4.32 (m, 4H), 4.51 (ABd, J_{AB} = 11.8 Hz, 1H), 4.65 (ABd, J_{AB} = 11.8 Hz, 1H), 4.73 (d, J = 11.4 Hz, 1H), 4.96 (t, J = 9.2 Hz, 1H), 5.00 (t, J = 9.3 Hz,1H), 5.03–5.11 (m, 2H), 5.30 (t, J = 9.8 Hz, 1H), 5.54 (d, J = 8.4 Hz, 1H), 5.98 (dd, J = 9.2 and 10.7 Hz, 1H), 6.63 (d, J = 9.8 Hz, 1H), 7.24–7.39 (m, 11H); MS FAB(+) *m/z* 1061 [(M+H)$^+$, 5]; HR-MS calcd for $C_{50}H_{65}N_2O_{23}Na$ [(M+H)$^+$] 1061.3978, found: 1061.3981.

4.1.24. 2,6-Di-*O*-[3,4,6-tri-*O*-acetyl-2-acetamido-2-deoxy-β-D-glucopyranosyl]-1,3,4-tri-*O*-acetyl-α-D-mannopyranose (29)

To an ethanol (10 mL) solution of **28** (118 mg, 0.11 mmol) was added Pd-C (10%, ca. 100 mg) and ammonium formate (140 mg). The reaction mixture was refluxed overnight, filtered through Celite® and concentrated in vacuo. The residue was dissolved in pyridine (2 mL) and acetic anhydride (2 mL) was added. The mixture was stirred overnight at room temperature and methanol (20 mL) was added. The solvent was removed, and the residue was purified by silica gel chromatography (chloroform/methanol = 20:1) to give **29** (78 mg, 72%, 2 steps). ^{1}H NMR (300 MHz, $CDCl_3$) δ: 1.97, 2.00, 2.01, 2.02, 2.05, 2.06, 2.06, 2.09, 2.11 and 2.12 (each s, 3H), 2.97–3.05 (m, 2H), 3.13–3.16 (m, 1H), 3.62–3.66 (m, 1H), 3.75–3.79 (m, 2H), 3.96–4.01 (m, 1H), 4.10–4.29 (m, 6H), 4.92 (t, J = 9.7 Hz, 1H), 5.06–5.10 (m, 4H), 5.45 (t, J = 9.7 Hz, 1H), 5.46 (d, J = 9.2 Hz, 1H), 5.90 (dd, J = 10.6 and 9.2 Hz, 1H, 6.05 (d, J = 1.8 Hz, 1H), 6.41 (d, J = 9.5 Hz, 1H), 7.23 (d, J = 3.9 Hz, 1H); MS FAB(+) *m/z* 965 [(M+H)$^+$, 5]; HR-MS calcd for $C_{40}H_{57}N_2O_{25}$ [(M+H)$^+$] 965.3250, found: 965.3255.

4.1.25. 2-(4-Iodophenyl)ethyl 6-*O*-[2,6-di-*O*-(3,4,6-tri-*O*-acetyl-2-acetamido-2-deoxy-β-D-glucopyranosyl)-3,4-di-*O*-acetyl-α-D-mannopyranosyl]-2,3,4-tri-*O*-acetyl-β-D-glucopyranoside (31)

To a solution of **29** (70 mg, 0.073 mmol) and acetic anhydride (1.5 mL) was added hydrogen bromide (30% in acetic acid, 3 mL). The mixture was stirred overnight at room temperature, poured into ice water, and extracted with chloroform. The organic layer was washed with water and a saturated sodium hydrogencarbonate solution, dried over sodium sulfate, filtered, and evaporated to give **30** (67 mg). To a solution of **4** (30 mg, 0.055 mmol), dichloromethane (1 mL), and toluene (1 mL) was added silver carbonate (17 mg, 0.06 mmol). The reaction mixture was stirred at room temperature for 1 h under a nitrogen atmosphere, and silver perchlorate (2 mg, 0.0082 mmol) was added. After stirring for 30 min at room temperature, a solution of **30** (65 mg, 0.066 mmol), dichloromethane (2 mL), and toluene (2 mL) was added and the mixture was stirred for another 15 h. After the reaction was completed, the mixture was filtered. The filtrate was concentrated in vacuo, and the residue was purified by silica gel chromatography (chloroform/methanol = 20:1) to afford **31** (5 mg, 7%, 2 steps). ^{1}H NMR (400 MHz, $CDCl_3$) δ: 1.87, 1.94, 1.96, 1.97, 1.99, 2.00, 2.03, 2.04, 2.05, 2.06, 2.08, 2.09, and 2.09 (each s, 3H), 2.82–2.96 (m, 3H), 3.06–3.09 (m, 1H), 3.55–3.58 (m, 1H), 3.63–3.73 (m, 5H), 3.77–3.82 (m, 1H), 3.98–4.01 (m, 1H), 4.09–4.32 (m, 8H), 4.45 (d, J = 8.1 Hz, 1H), 4.82 (d, J = 1.5 Hz, 1H), 4.88–4.98 (m, 3H), 5.02–5.10 (m, 3H), 5.17 (t, J = 9.5 Hz, 1H), 5.35 (t, J = 9.6 Hz, 1H), 5.38 (d, J = 8.2 Hz, 1H), 5.92 (dd, J = 10.8 and 9.2 Hz, 1H), 6.43 (d, J = 9.9 Hz, 1H), 6.95–6.97 (m, 2H), 7.30 (d, J = 7.0 Hz, 1H), 7.56–7.59 (m, 2H); MS FAB(+) *m/z* 1463 [(M+Na)$^+$, 5]; HR-MS calcd for $C_{58}H_{77}N_2O_{32}I$ [(M+Na)$^+$] 1463.3402, found: 1463.3394.

4.1.26. 2-(4-Iodophenyl)ethyl 6-*O*-[2,6-di-*O*-(2-acetamido-2-deoxy-β-D-glucopyranosyl)-α-D-mannopyranosyl]-β-D-glucopyranoside (IPGGMG, 2)

To a methanol (1 mL) solution of **31** (13 mg, 0.009 mmol) was added sodium methoxide (28% in methanol, 10 μL, 0.050 mmol) and the mixture was stirred at room temperature for 30 min. After the reaction was completed, the mixture was neutralized with Amberlyst® 15 (ca. 100 mg) and filtered. The filtrate was concentrated in vacuo to afford **2** (5 mg, 57%). ^{1}H NMR (400 MHz, CD_3OD) δ: 2.02, 2.06 (each s, 3H), 2.85–2.93 (m, 2H), 3.12–3.19 (m, 1H), 3.24–3.38 (m, 8H), 3.45–3.76 (m, 11H), 3.84–3.89 (m, 3H), 3.96 (br s, 1H), 4.01–4.10 (m, 2H), 4.28 (d, J = 7.7 Hz, 1H), 4.45 (d, J = 8.2 Hz, 1H), 4.58 (d, J = 7.7 Hz, 1H), 4.80 (s, 1H), 7.06–7.09 (m, 2H), 7.59–7.61 (m, 2H); MS FAB(+) *m/z* 1001 [(M+Na)$^+$, 2]; HR-MS calcd for $C_{36}H_{55}O_{21}N_2INa$ [(M+Na)$^+$] 1001.2240, found: 1001.2245.

4.2. Iododestannylation Reaction

The radiolabeled compound [^{125}I]**20** was prepared from the corresponding tributyltin derivative **21** by iododestannylation. Briefly, to initiate the reaction, 10 μL of H_2O_2 (5%) was added to a mixture of a tributyltin derivative (100 μg/100 μL MeOH), 0.2 mCi sodium [^{125}I]iodide, and 20 μL of 0.1 N HCl in a sealed vial. The reaction was allowed to proceed at room temperature for 30 min. The reaction mixture was neutralized with sodium bicarbonate, and extracted with ethyl acetate. The extract was evaporated and methanol (100 μL) was added. To the solution was added sodium methoxide (28% in methanol, 1.6 μL). The reaction mixture was stirred at room temperature for 45 min, and neutralized with Amberlyst® 15. The residue was purified by HPLC on a Cosmosil 5C18 AR-300 column (4.6×150 mm) with an isocratic solvent of H_2O/acetonitrile (83/17) at a flow rate of 1.0 mL/min.

4.3. Enzymatic Reactions of Radioiodinated IPGMG

GnT-V-transfected WiDr cells were used as the enzyme source. The protein concentration was measured by the Lowry method.[23] Lysate of GnT-V-overexpressing WiDr cells was incubated with MES buffer (125 mM, pH 6.25) containing 40 mM UDP-GlcNAc, 200 mM GlcNAc, 0.5% Triton X-100, and 10 mM EDTA for 10 min at 37 °C. [^{125}I]IPGMG was then added, and the incubation continued for an additional 4 h. The reaction was stopped by heating at 100 °C for 1 min. Enzymatic products were analyzed by HPLC on a TSK-GEL ODS-80TM column (4.6×150 mm) with an isocratic solvent of H_2O/acetonitrile (85/15) at a flow rate of 1.0 mL/min.

4.4. GnT-V Activities in Rat Tissues

Animal experiments were conducted in accordance with our institutional guidelines, and the experimental procedures were approved by the Kyoto University Animal Care Committee. Various tissues from male Wistar rats weighing 240–260 g were homogenized in 4 volumes of 10 mM Tris-HCl buffer (pH 7.4) containing 0.25 M sucrose. After centrifugation at 900 × g for 10 min, the supernatants were collected and used as crude enzyme preparations. The GnT-V activity and protein concentration were determined according to the procedures described above.

References

1. Cummings, R. D.; Trowbridge, I. S.; Kornfeld, S. J. *Biol. Chem.* **1982**, *257*, 13421–13427.
2. Yamashita, K.; Tachibana, Y.; Ohkura, T.; Kobata, A. J. *Biol. Chem.* **1985**, *260*, 3963–3969.
3. Pierce, M.; Arango, J. *J. Biol. Chem.* **1986**, *261*, 10772–10777.
4. Dennis, J. W.; Laferte, S.; Waghorne, C.; Breitman, M. L.; Kerbel, R. S. *Science* **1987**, *236*, 582–585.
5. Dennis, J. W.; Laferte, S. *Cancer Res.* **1989**, *49*, 945–950.
6. Fernandes, B.; Sagman, U.; Auger, M.; Demetrio, M.; Dennis, J. W. *Cancer Res.* **1991**, *51*, 718–723.
7. Miyoshi, E.; Nishikawa, A.; Ihara, Y.; Gu, J.; Sugiyama, T.; Hayashi, N.; Fusamoto, H.; Kamada, T.; Taniguchi, N. *Cancer Res.* **1993**, *53*, 3889–3992.
8. Murata, K.; Miyoshi, E.; Kameyama, M.; Ishikawa, O.; Kabuto, T.; Sasaki, Y.; Hiratsuka, M.; Ohigashi, H.; Ishiguro, S.; Ito, S.; Honda, H.; Takemura, F.; Taniguchi, N.; Imaoka, S. *Clin. Cancer Res.* **2000**, *6*, 1772–1777.
9. Dennis, J. W.; Pawling, J.; Cheung, P.; Partridge, E.; Demetriou, M. *Biochim. Biophys. Acta* **2002**, *157*, 414–422.
10. Saito, T.; Miyoshi, E.; Sasai, K.; Nakano, N.; Eguchi, H.; Honke, K.; Taniguchi, N. *J. Biol. Chem.* **2002**, *277*, 17002–17008.
11. Pierce, M.; Arango, J.; Tahir, S. H.; Hindsgaul, O. *Biochem. Biophys. Res. Commun.* **1987**, *146*, 679–684.
12. Brockhausen, I.; Reck, F.; Kuhns, W.; Khan, S.; Matta, K. L.; Meinjohanns, E.; Paulsen, H.; Shah, R. N.; Baker, M. A.; Schachter, H. *Glycoconj. J.* **1995**, *12*, 371–379.
13. Nishikawa, A.; Gu, J.; Fuji, S.; Taniguchi, N. *Biochim. Biophys. Acta* **1990**, *1035*, 313–318.
14. Taniguchi, N.; Nishikawa, A.; Fuji, S.; Gu, J. *Methods Enzymol.* **1989**, *179*, 397–408.
15. Sasai, K.; Ikeda, Y.; Tsuda, T.; Ihara, H.; Korekane, H.; Shiota, K.; Taniguchi, N. *J. Biol. Chem.* **2001**, *276*, 759–765.
16. Srivastava, O. P.; Hindsgaul, O.; Shoreibah, M.; Pierce, M. *Carbohydr. Res.* **1988**, *179*, 137–161.
17. Linker, T.; Crawley, S. C.; Hindsgaul, O. *Carbohydr. Res.* **1993**, *245*, 323–331.
18. Palcic, M. M.; Pierce, M.; Hindsgaul, O. *Methods Enzymol.* **1994**, *247*, 215–227.
19. Goodman, M. M.; Kirsch, G.; Knapp, F. F., Jr. *J. Med. Chem.* **1984**, *27*, 390–397.
20. Boger, D. L.; Honda, T. *J. Am. Chem. Soc.* **1994**, *116*, 5647–5656.
21. Akiya, S.; Oshawa, T. *Yakugaku Zasshi* **1957**, *77*, 726–730.
22. Tamara, T.; Kuromatsu, K.; Suwa, K.; Koizumi, K.; Shingu, T. *Chem. Pharm. Bull.* **1986**, *34*(6), 2341–2353.
23. Lowry, O. H.; Rosebrough, N. J.; Farr, A. L.; Randall, R. J. *J. Biol. Chem.* **1951**, *193*, 265–275.